J. Astrophys. Astr.(1984) **5,** 429–473

Extragalactic Sources with Asymmetric Radio Structure I. Observations of 17 Sources.

D. J. Saikia & P. Shastri *Radio Astronomy Centre, Tata Institute of Fundamental Research, Post Box 1234, Bangalore 560012*

R. P. Sinha *Systems and Applied Science Corporation, 5809 Annapolis Road, Hyattsville, MD 20784, USA*

V. K. Kapahi *Radio Astronomy Centre, Tata Institute of Fundamental Research, Post Box 1234, Bangalore 560012*

G. Swarup *Radio Astronomy Centre, Tata Institute of Fundamental Research, Post Box 8, Udhagamandalam 643001*

Received 1984 April 17; accepted 1984 June 8

Abstract. We present total-intensity and linear-polarization observations with the Very Large Array (VLA) at λ6 and 2 cm of 17 sources, almost all of which were suspected to have extended emission only on one side of the nucleus. Five of them are still one-sided, three appear unresolved, while seven have radio lobes on both sides of the nucleus. The outer components in the double-lobed sources, however, have significantly different surface brightness or are very asymmetrically located with respect to the nucleus.

Key words: extragalactic radio sources—asymmetric radio structure—linear polarization

1. Introduction

The vast majority of powerful, extended, extragalactic radio sources have relatively symmetric double structure with lobes on opposite sides of the optical or nuclear component. However, a small fraction show highly asymmetric structure having a compact component coincident with the optical object and a single extended lobe on one side. These sources are often referred to as D2-type (Miley 1971) double sources. A list of 49 such objects was compiled by Kapahi (1981a; hereafter referred to as K 81). This class of sources does not include the relatively lower luminosity ($P_{178} \lesssim 2 \times 10^{25}$ W Hz^{-1} sr^{-1}) head-tail radio sources generally found in clusters of galaxies, although these often show one-sided radio structure. The large majority of sources in the K 81 list are identified with quasars or blue stellar objects.

Most of the sources listed by K 81 were identified to be one-sided from observations made with either the Westerbork telescope, the NRAO interferometer or the Cambridge 5-km array. To confirm their classification from observations with better resolution and sensitivity, we have observed a large number of sources from the K 81 list with the Very Large Array (VLA). A systematic study of the properties of those which still appear one-sided and possible explanations for their observed morphology

Table 1. The list of sources.

Source	Alternative name	Optical Identification	Optical position						Ref. for position	Redshift	LAS
			Right Ascension			Declination					(arcsec)
			h	m	s	°	′	″			
(1)	(2)	(3)		(4)			(5)		(6)	(7)	(8)
0232 − 042	4C − 04.06	Q	02	32	36.550	−04	15	10.24	C83	1.436	13.2
0309 + 411	NRAO 128	G	03	09	44.81	41	08	48.9	EKM		u
0717 + 170	3C 176	U									105.7
0740 + 380	3C 186	Q	07	40	56.817	38	00	31.04	C83	1.063	100.4
0742 + 376	4C 37.19	BSO	07	42	22.63	37	38	33.6	P		62.3
0821 + 394	4C 39.23A	Q	08	21	37.26	39	26	28.0	PW	1.216	u
0836 + 195	4C 19.31	Q	08	36	15.00	19	32	24.4	MH	1.691	31.2
0932 + 022	4C 02.27	Q	09	32	42.93	02	17	39.6	MH	0.659	44.8
1007 + 417	4C 41.21	Q	10	07	26.13	41	47	24.4	C77	0.611	32.0
1047 + 096	4C 09.37	Q	10	47	48.95	09	41	47.7	MH	0.786	21.1
1055 + 201	4C 20.24	Q	10	55	37.59	20	07	55.3	MH	1.110	21.2
1320 + 299	4C 29.48	BSO	13	20	40.47	29	57	23.2	F79		51.4
1347 + 539	4C 53.28	BSO	13	47	42.66	53	56	08.0	C77		u
1354 + 195	4C 19.44	Q	13	54	42.14	19	33	42.6	MH	0.720	43.7
1419 + 315	4C 31.45	BSO	14	19	19.39	31	32	43.7	F79		13.1
1636 + 473	4C 47.44	Q	16	36	19.17	47	23	28.7	P	0.740	20.0
1729 + 501	4C 50.43	Q	17	29	49.26	50	09	44.3	C77	1.107	20.4

References:

C77	Cohen *et al.* (1977)	MH	Miley & Hartsuijker (1978)
C83	Clements (1983)	P	Present work
EKM	Edwards, Kronberg & Menard (1975)	PW	Potash & Wardle (1979)
F79	Fanti *et al.* (1979b)		

will be discussed in a forthcoming paper. The present paper, which is the first of a series, describes C-array observations of all but three of the sources inthe K81 list with largest angular sizes $\geqslant$ 5 arcsec. Two sources were omitted as they had been already studied with high resolution and sensitivity. These are 3C 273 (Perley 1981; Conway *et al.* 1981) and 3C293 (Bridle, Fomalont & Corn well 1981). Bridle, Fomalont & Cornwell have shown that 3C293, a galaxy, is not truly one-sided, but has an extremely asymmetric brightness distribution. The third source not included in the present set of observations is 2041 – 149. To the remaining sample of 14 sources were added the QSOs 0232 – 042 Mley & Hartsuijker 1978; hereinafter MH78) and 1007 + 417 (Kapahi 1981b), and the radio source 3C176 (Joshi 1981), all of which were suspected of having one-sided radio structure and angular sizes $\gtrsim$ 15 arcsec.

The final list of 17 sources is presented in Table 1, which is arranged as follows.

Columns 1 and 2: The source name in the coordinate designation, together with an alternative name.

Column 3: Optical identification; Q: quasar, G: galaxy, BSO: blue stellar object, U: unidentified.

Columns 4, 5 and 6: Position of the optical object (epoch 1950) and a reference for the position.

Column 7: Redshift The values are from Hewitt & Burbidge (1980).

Column 8: The largest angular size (LAS) of the radio structure in arcsec; u: unresolved. These values are from the present observations.

The VLA observations possess sufficient resolution to give at least three beamwidths across each source at a wavelength of 6 cm. The sensitivity of the observations permitted fairly good dynamic ranges to be obtained. This was of particular importance to check if a much weaker outer component (hereinafter referred to as OC) was present on the opposite side of the nucleus in addition to the dominant OC.

2. Observations and analyses

The present observations were made on 1980 July 13 and 14, and were among the first made with the completed VLA (Thompson *et al.* 1980). The array was in its C configuration giving a maximum baseline of about 3.4 km. Observations were made at *C* band (λ6 cm) and *U* band (λ2 cm). The observational parameters of the system are shown in Table 2.

For each source, ten-minute observations were made at a number of hour angles (typically three) at each frequency. The *C*- and U-band observations were interleaved

Table 2. Parameters of the observations.

	λ6 cm	λ2 cm
Frequency (MHz)	4885	15035
Bandwidth (MHz)	50	50
System temperature (K)	60	300
Typical HPBW (arcsec)	5	1.5
Typical largest structure 'visible' (arcsec)	125	40
Typical number of antennas available	23	22

Table 3. Flux densities of secondary calibrators.

Source	S_{4885} (Jy)	S_{15035} (Jy)
0316 + 161	2.95	0.71
0316 + 413	57.0	51.3
0711 + 356	1.10	0.47
0839 + 187	0.97	0.53
1404 + 286	2.90	1.41
1739 + 522	0.92	1.05

with the calibrators which were observed about every twenty-five minutes. 3C 286 was the primary calibrator with assumed flux densities of 7.41 Jy at λ6 cm and 3.48 Jy at λ2 cm. Six secondary calibrators were used and their derived flux densities are given in Table 3.

The data were edited and calibrated via standard VLA DEC-10 computer programmes. Initial total power maps were made from the untapered visibility data and CLEANed on the PDP 11/70 system. Although the data were not tapered, attenuation due to bandwidth smearing is not significant for any of the sources in the present sample. The data were further processed using a self-calibration technique to minimize random phase errors (Schwab 1980). At *U* band, the highly extended source 3C176 had insufficient signal-to-noise ratio to permit the use of self-calibration.

The linear polarization characteristics of the sources were also mapped at both frequencies using 3C286 as a calibrator, for which a polarization percentage of 11.3 at position angle (PA) 33° was adopted at *C* band and 11.6 at 33° at *U* band. Correction for the instrumental polarization was made using the extensive observations of the secondary calibrators. To obtain the most accurate possible estimates of polarization percentages on the sources, a further set of total power maps was made using only those baselines for which polarization information was available.

3. Results

The λ6- and 2-cm observational parameters for the individual sources are given in Table 4. For each source at each frequency, the root-mean-square (rms) noises on the final total power and polarization maps are given, along with the half-power beamwidths (HPBW)and orientations of the restored elliptical Gaussian beams used in the CLEAN process.

The self-calibrated total power maps of the sources are shown in Figs 1–14. The figures have not been corrected for attenuation by the primary polar diagram. The maps for the sources 0309 + 411, 0821 + 394 and 1347 + 539 are not included as they showed only a point source coincident with the optical object. For the same reason the λ2-cm map of 1354 + 195 is not reproduced. Also shown in the figures are the λ6-cm maps of linear polarization. Vectors representing polarized intensity are superposed on total power contours containing information only from those baselines which possessed polarization information (see Section 2). When considering the total power structures of the sources at λ6 cm, Figs l(a) to 14(a) should be used exclusively. Due to insufficient signal-to-noise ratio at λ2 cm all components showing linear polarization at

Table 4. The observational parameters for individual sources.

Source	λ6 cm					λ2 cm				
	σ_{tp} (mJy/ beam)	σ_{pol} (mJy/ beam)	HPBW major (″)	HPBW minor (″)	PA (°)	σ_{tp} (mJy/ beam)	σ_{pol} (mJy/ beam)	HPBW major (″)	HPBW minor (″)	PA (°)
0232 − 042	2.3	0.3	5.24	3.94	171	1.7	3.4	1.77	1.42	19
0309 + 411	1.0	0.2	4.96	3.88	72	2.3	2.2	1.65	1.27	71
0717 + 170	0.4	0.6	5.36	4.28	55	1.7	2.4	1.68	1.51	70
0740 + 380	0.9	0.2	5.00	3.96	95	1.2	2.4	1.70	1.33	92
0742 + 376	0.8	0.2	5.21	3.98	95	1.4	2.1	1.77	1.36	95
0821 + 394	6.4	0.4	4.59	4.32	82	8.1	2.5	1.96	1.40	100
0836 + 195	0.3	0.2	4.72	4.37	98	1.1	1.6	1.53	1.48	75
0932 + 022	0.6	0.2	6.15	4.75	116	1.2	2.6	1.65	1.34	30
1007 + 417	0.9	0.2	4.84	3.95	104	1.4	2.3	1.57	1.29	85
1047 + 096	0.3	0.3	4.67	4.14	175	1.1	1.9	1.53	1.37	17
1055 + 201	3.1	0.3	4.37	4.01	16	6.6	2.5	1.48	1.31	176
1320 + 299	1.2	0.2	4.74	4.09	58	1.7	1.9	1.54	1.34	51
1347 + 539	1.8	0.2	4.88	3.84	106	2.6	3.9	1.66	1.27	125
1354 + 195	2.7	0.6	4.40	4.24	175	4.5	3.7	1.56	1.41	2
1419 + 315	0.8	0.2	4.42	3.91	63	1.1	1.9	1.51	1.35	50
1636 + 473	0.8	0.2	4.32	3.77	97	2.9	1.6	1.61	1.22	70
1729 + 501	1.0	0.6	4.44	3.87	71	1.3	1.8	1.43	1.23	68

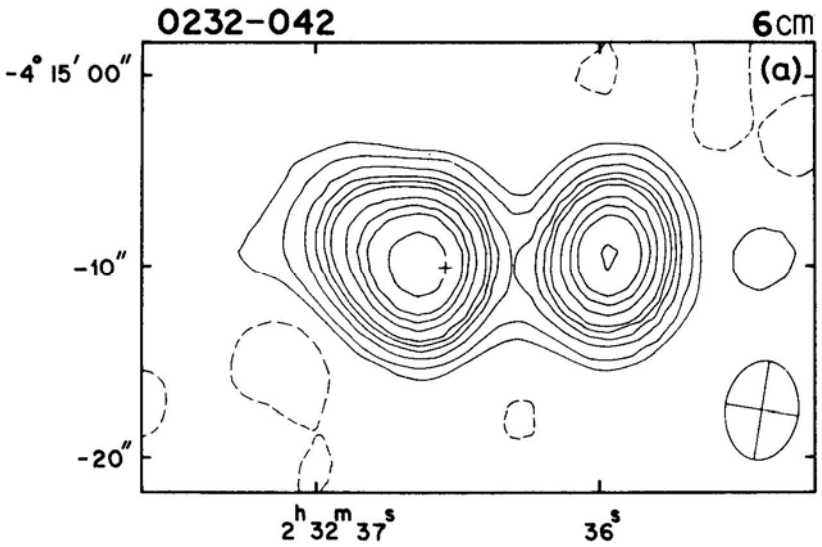

Figure 1.·* (a) 0232–042. Contours: 230 × (–0.04, –0.02, 0.02, 0.04, 0.08, 0.12, 0.16, 0.20, 0.30, 0.40,0.50, 0.75).

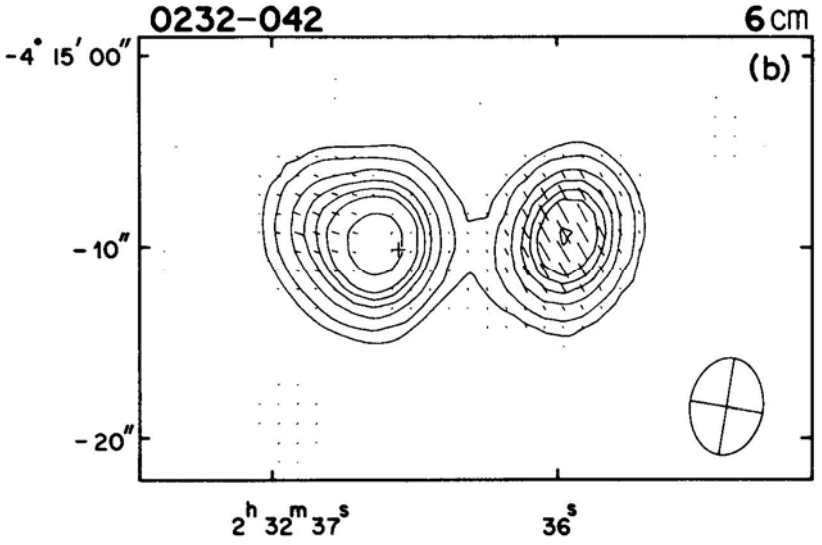

Figure 1. (b) 0232–042. Contours: 240 × (–0.10, –0.05, 0.05, 0.10, 0.20, 0.30, 0.40, 0.50, 0.75).

* In Figs 114, the crosses mark the positions of the optical objects while the ellipses indicate the sizes of the CLEAN beams listed in Table 4. Contours are listed as fractions of the peak flux density on the map in units of mJy/beam. The figures have not been corrected for attenuation by the primary polar diagram. The flux density values corrected for attenuation are listed in Tables 5a and 5b. The λ6–cm total-power maps using data from all baselines are shown in Figs l(a) to 14(a), while total-power contours containing information only from those baselines which possessed polarization information are shown in Figs l(b) to 14(b). In these figures, vectors representing polarized intensity are superposed on the total-power contours. The λ2 cm maps are shown in Figs l(c) to 14(c).

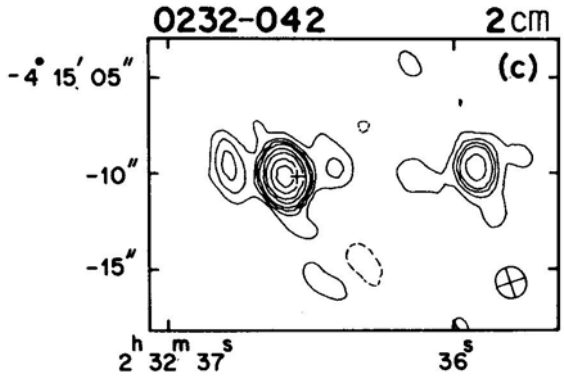

Figure 1. (c) 0232–042. Contours: 121 × (–0.06, –0.03, 0.03, 0.06, 0.09, 0.12, 0.20, 0.30, 0.50, 0.75).

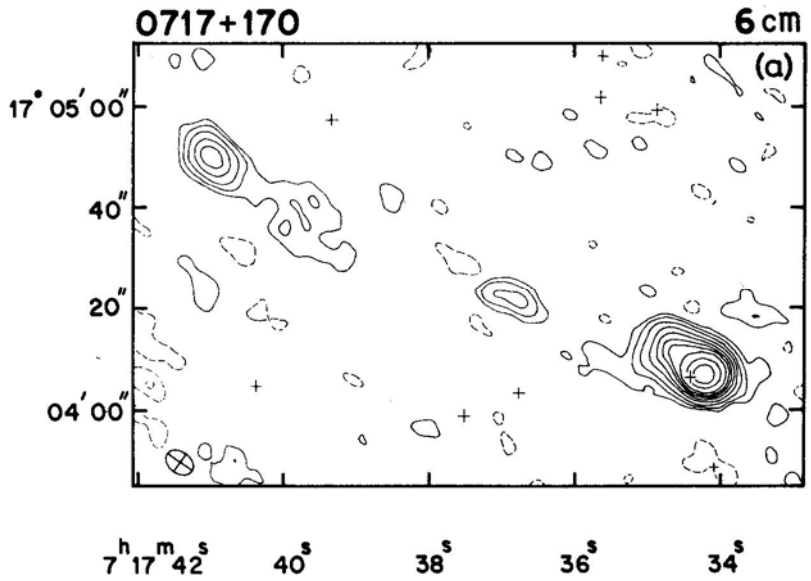

Figure 2. (a) 0717 +170. Contours: 101 × (–0.015, –0.0075, 0.0075, 0.015, 0.03, 0.06, 0.10, 0.15, 0.20, 0.30, 0.50, 0.75).

a 2σ or higher level were either unresolved, or only marginaly resolved. The $\lambda 2$ cm maps of linear polarization are therefore not included and the relevant information can be found in Table 5b.

The detailed information on the individual objects at $\lambda 6$ cm is to be found in Table 5a, with the corresponding data for $\lambda 2$ cm being contained in Table 5b. Table 5a is arranged as follows.

Column 1: The source name.

Column 2: Sub-component identification.

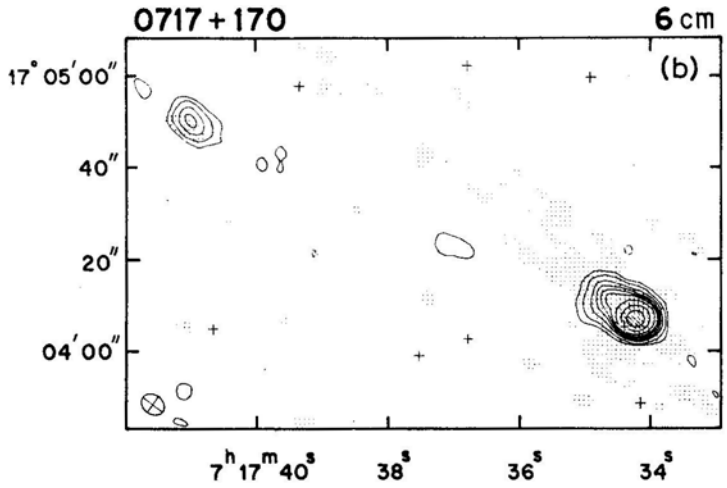

Figure 2. (b) 0717 +170, entire source. Contours: 94 × (–0.04, –0.02, 0.02, 0.04, 0.08, 0.12, 0.16, 0.20, 0.30, 0.50, 0.75).

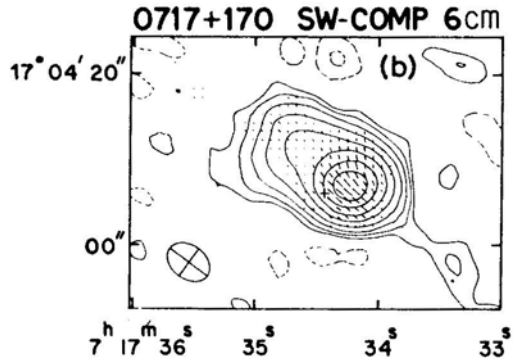

Figure 2. (b) 0717 +170, southwestern component. Contours: 94 × (–0.02, –0.01, 0.01, 0.02, 0.04, 0.08, 0.16, 0.30, 0.50, 0.75).

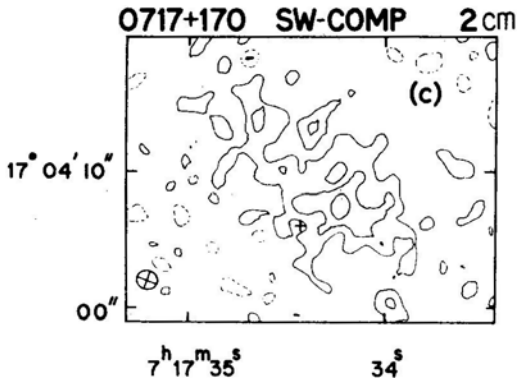

Figure 2. (c) 0717 +170. Contours: 12 × (–0.50, –0.25, 0.25, 0.50, 0.75).

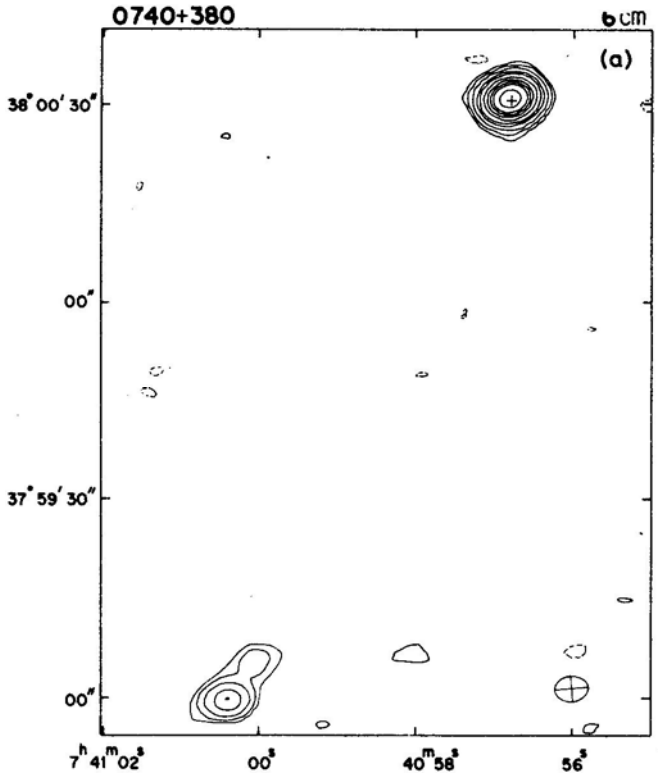

Figure 3. (a)0740 + 380. Contours: 210 × (–0.02, –0.01, 0.01, 0.02, 0.04, 0.08, 0.12, 0.20, 0.30, 0.40, 0.50, 0.75).

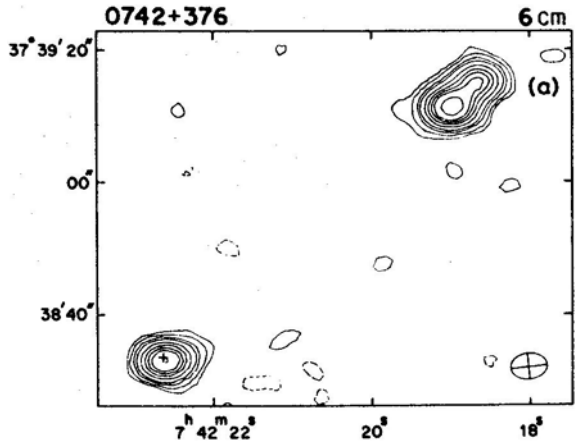

Figure 4. (a) 0742 + 376. Contours: 76 × (–0.04, –0.02, 0.02, 0.04, 0.08, 0.12, 0.20, 0.30, 0.40, 0.50,0.75).

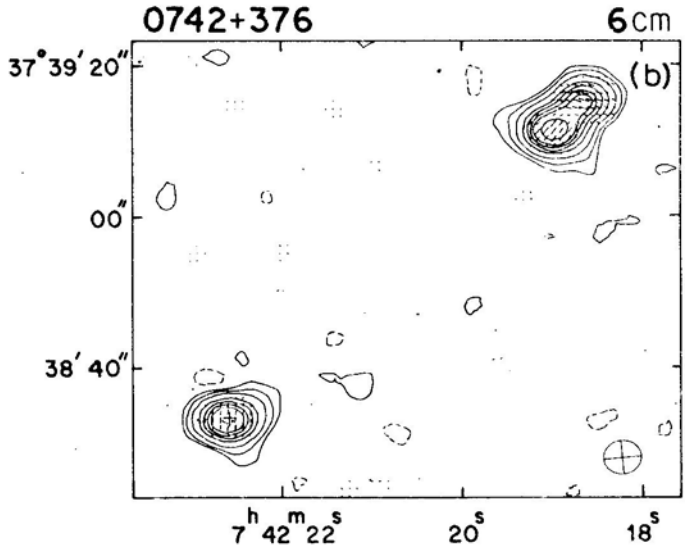

Figure 4. (b) 0742 + 376. Contours: 72 × (0.05, 0.025, 0.025, 0.05, 0.10, 0.20, 0.30, 0.40, 0.50, 0.75).

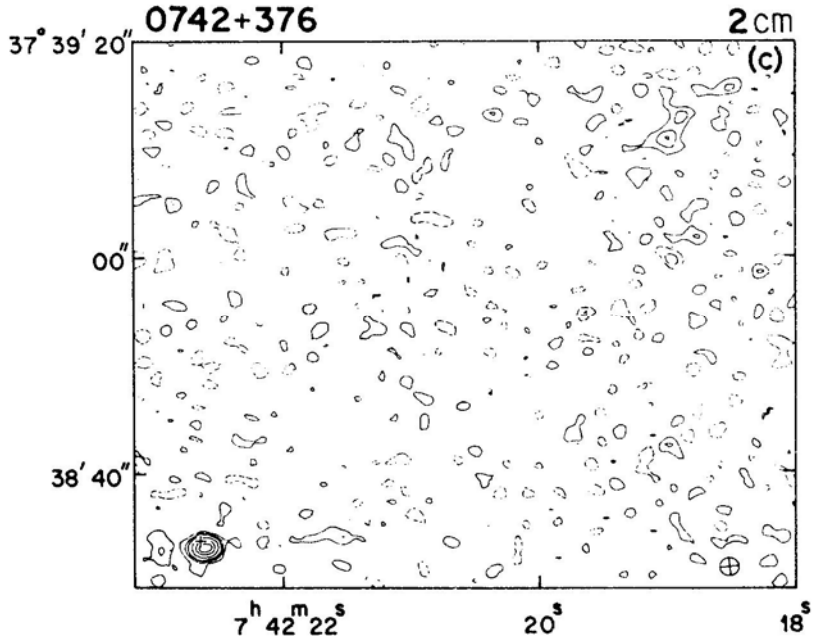

Figure 4. (c) 0742 + 376. Contours: 47 × (–0.10, –0.05, 0.05, 0.10, 0.15, 0.30, 0.50, 0.75).

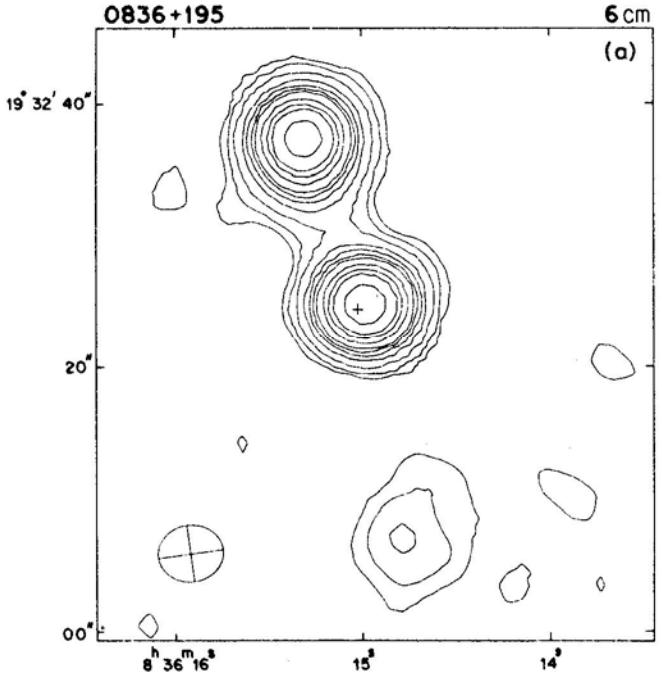

Figure 5. (a) 0836 + 195. Contours: 71 × (–0.02, –0.01, 0.01, 0.02, 0.04, 0.08, 0.12, 0.16, 0.20, 0.30, 0.40, 0.50, 0.75).

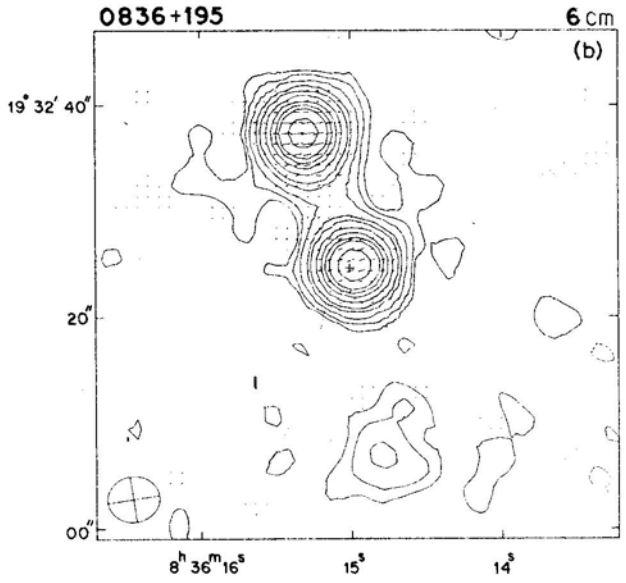

Figure 5. (b) 0836 +195. Contours: **72 × (–**0.02, –0.01, 0**.**01**,** 0.02, 0.04, 0.08, 0.12, 0.20, 0.30, 0.40, 0.50, 0.75).

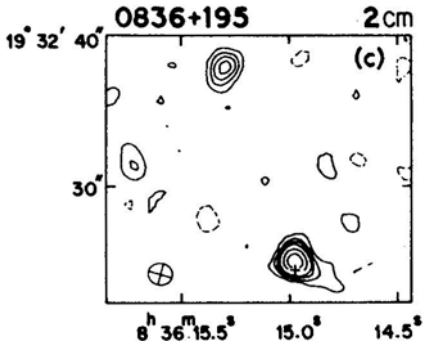

Figure 5. (c) 0836+195. Contours: 28 × (–0.15, –0.075, 0.075, 0.15, 0.225, 0.30, 0.50, 0.75).

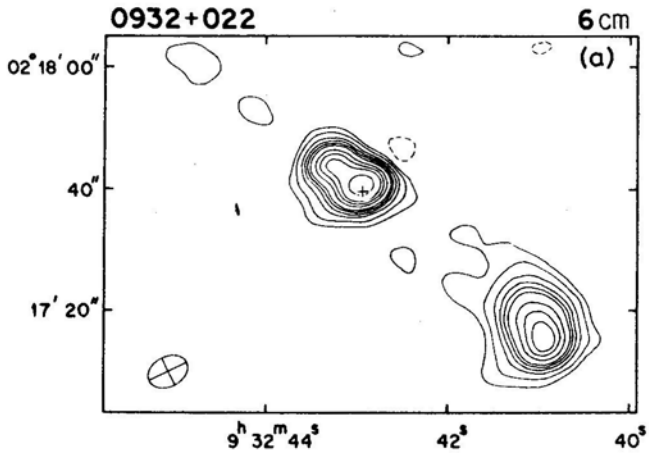

Figure 6. (a) 0932 + 022. Contours: 82 × (–0.04, –0.02, 0.02, 0.04, 0.08, 0.12, 0.16, 0.20, 0.30, 0.40, 0.50, 0.75).

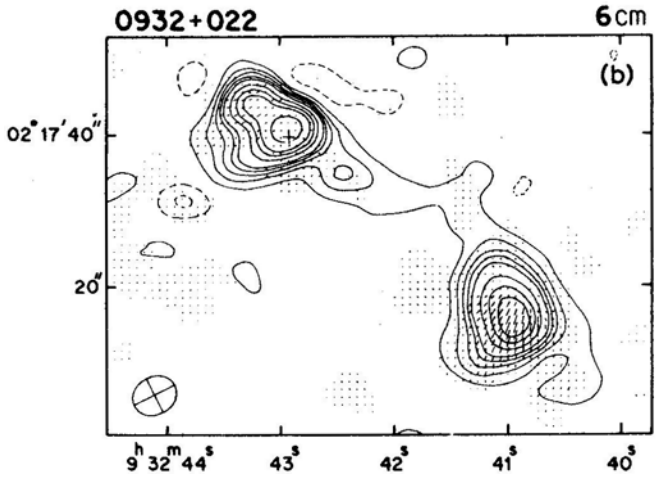

Figure 6. (b) 0932 + 022. Contours: 72 × (– 0.08, –0.04, 0.04, 0.08, 0.12, 0.16, 0.20, 0.30, 0.40, 0.50, 0.75)

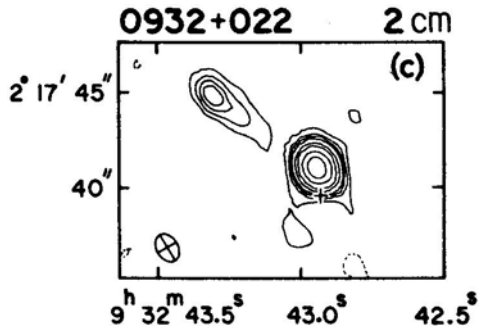

Figure 6. (c) 0932 + 022. Contours: 72 × (–0.06, –0.03, 0.03, 0.06, 0.09, 0.12, 0.20, 0.30, 0.50, 0.75).

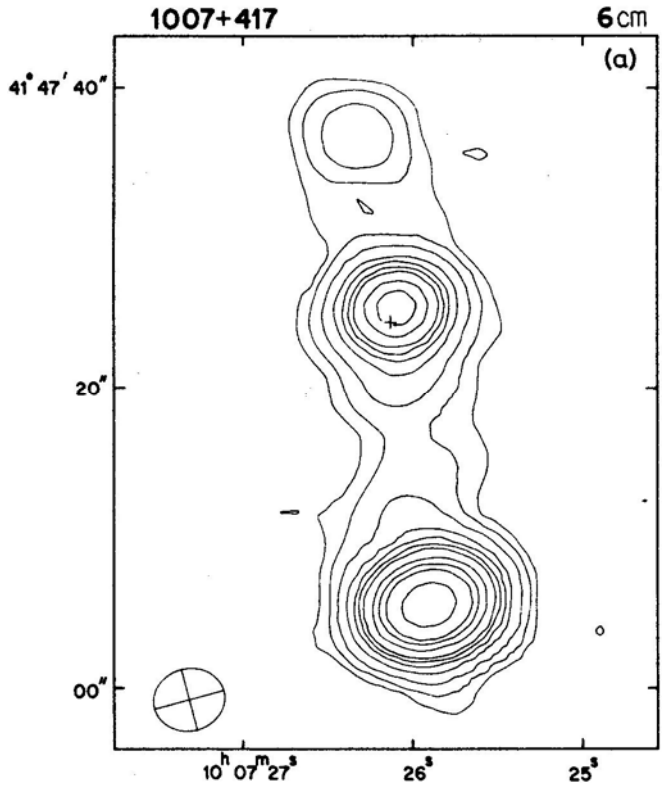

Figure 7. (a) 1007 + 417. Contours: 304 × (–0.02, –0.01, 0.01, 0.02, 0.04, 0.08, 0.12, 0.16, 0.20, 0.30, 0.40, 0.50, 0.75).

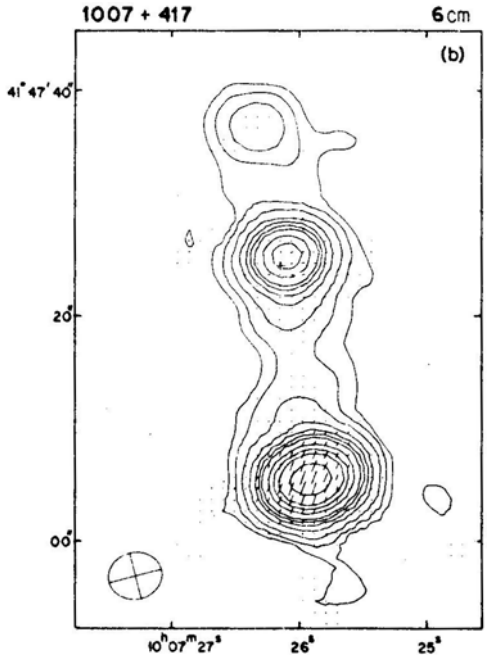

Figure 7. (b) 1007 + 417. Contours: 302 × (–0.02, –0.01, 0.01, 0.02, 0.04, 0.08, 0.12, 0.16, 0.20, 0.30, 0.40, 0.50, 0.75).

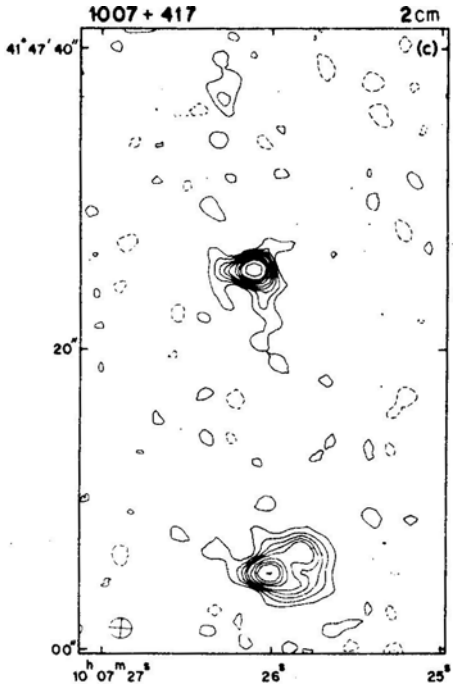

Figure 7. (c) 1007 + 417. Contours: 67 × (–0.08, –0.04, 0.04 0.08, 0.12, 0.16, 0.20, 0.30, 0.40, 0.50, 0.75).

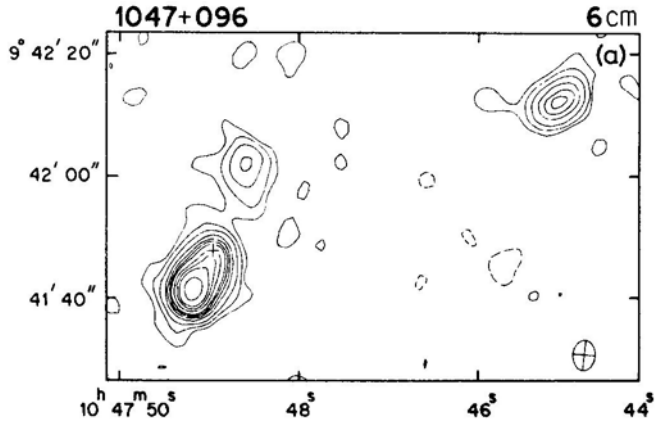

Figure 8. (a) 1047 + 096. Contours: 59 × (–0.02, –0.01, 0.01, 0.02, 0.04, 0.08, 0.12, 0.16, 0.20, 0.30, 0.40, 0.50, 0.75).

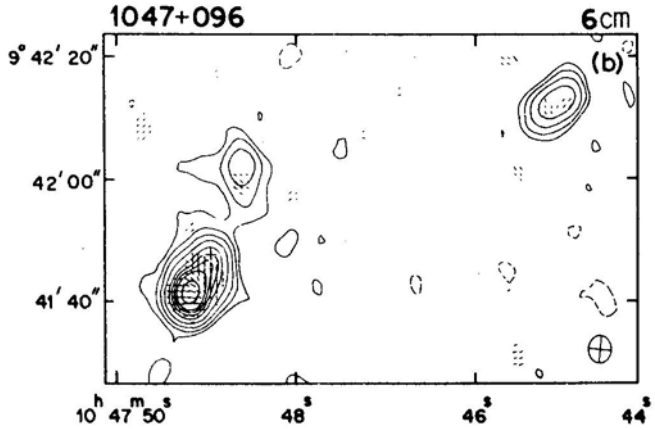

Figure 8. (b) 1047 + 096. Contours: 58 × (–0.025, –0.0125, 0.0125, 0.025, 0.05, 0.10, 0.20, 0.30, 0.40, 0.50, 0.75).

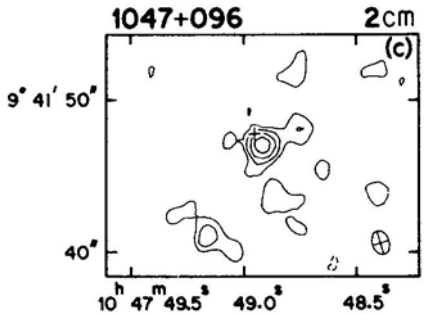

Figure 8. (c) 1047 + 096. Contours: 16 × (–0.30, –0.15, 0.15, 0.30, 0.50, 0.75).

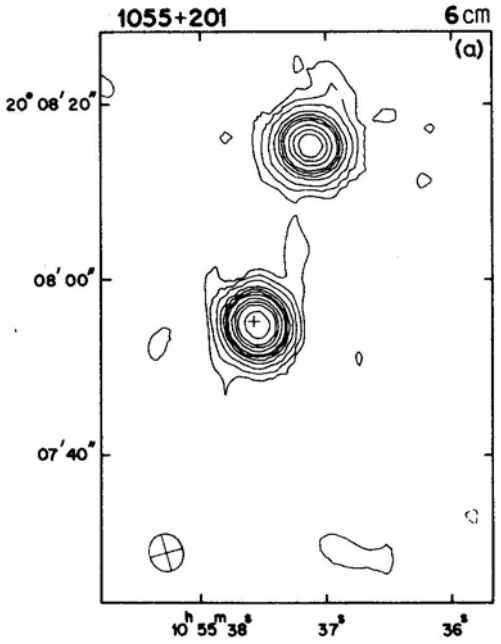

Figure 9. (a) 1055 + 201. Contours: 792 × (–0.02, –0.01, 0.01, 0.02, 0.04, 0.08, 0.12, 0.16, 0.20, 0.30, 0.40, 0.50, 0.75).

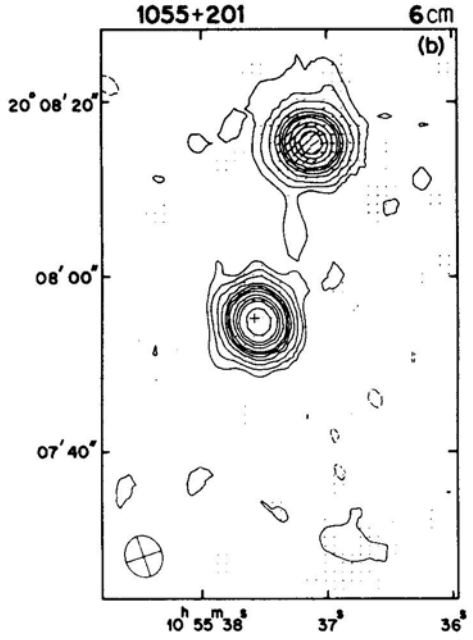

Figure 9. (b) 1055 + 201. Contours: 787 × (–0.02, –0.01, 0.01, 0.02, 0.04, 0.08, 0.12, 0.16, 0.20, 0.30, 0.40, 0.50, 0.75).

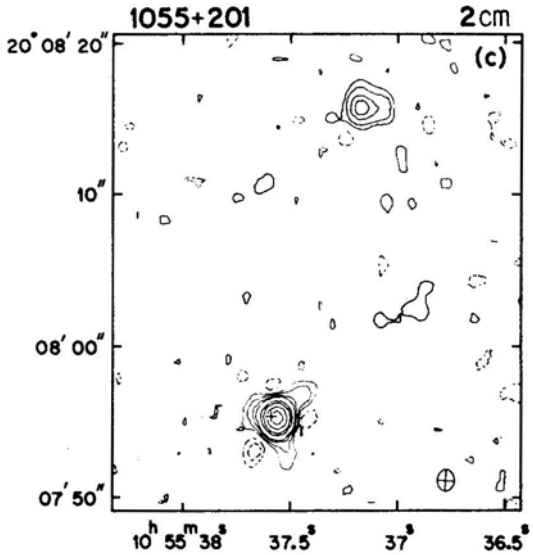

Figure 9. (c) 1055 + 201. Contours: 819 × (–0.03, –0.015, 0.015, 0.03, 0.06, 0.09, 0.20, 0.30, 0.50, 0.75).

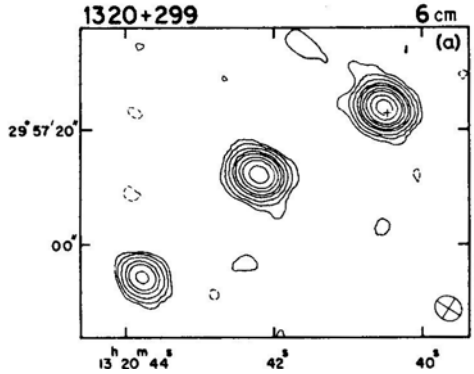

Figure 10. (a) 1320+299. Contours: 277 × (–0.02, –0.01, 0.01, 0.02, 0.04, 0.08, 0.12, 0.20, 0.30, 0.50, 0.75).

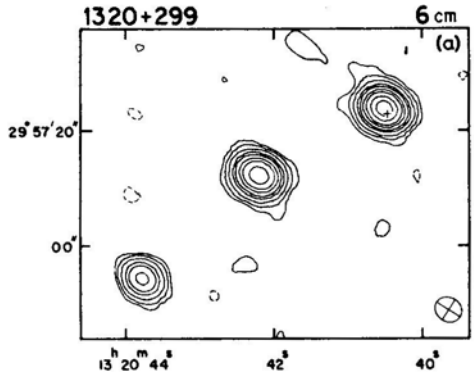

Figure 10. (b) 1320 + 299. Contours: 277 x (—0.02, —0.01, 0.01, 0.02, 0.04, 0.08, 0.12, 0.16, 0.20, 0.30, 0.40, 0.50, 0.75).

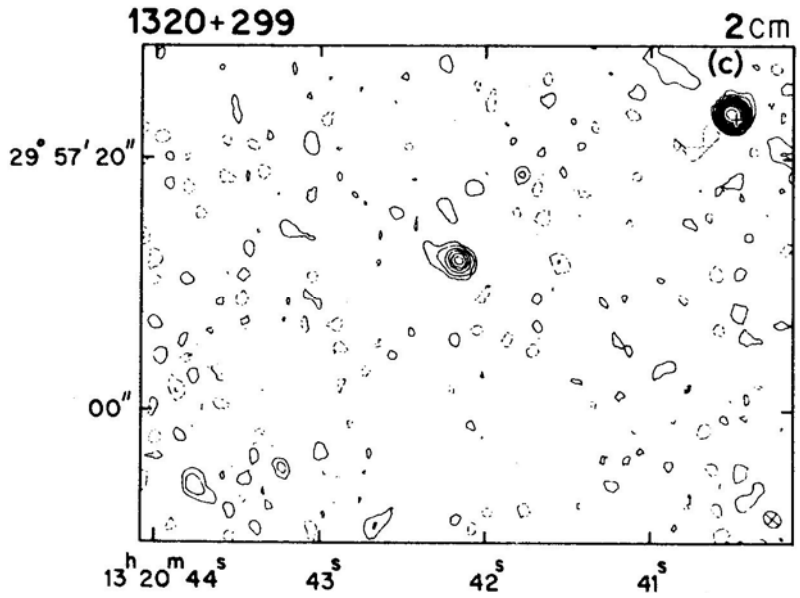

Figure 10. (c) 1320 + 299. Contours: 156 × (–0.04, –0.02, 0.02, 0.04, 0.08, 0.12, 0.16, 0.20, 0.30, 0.40, 0.50, 0.75).

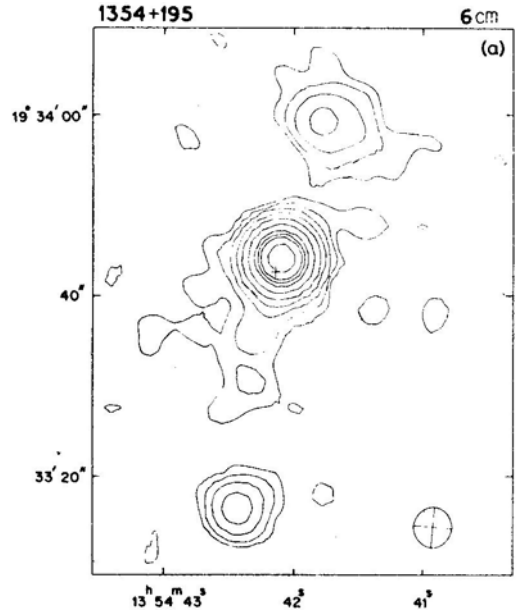

Figure 11. (a) 1354 + 195. Contours: 1229 × (–0.01, – 0.005, 0.005, 0.01, 0.02, 0.04, 0.08, 0.16, 0.30, 0.40, 0.50, 0.75).

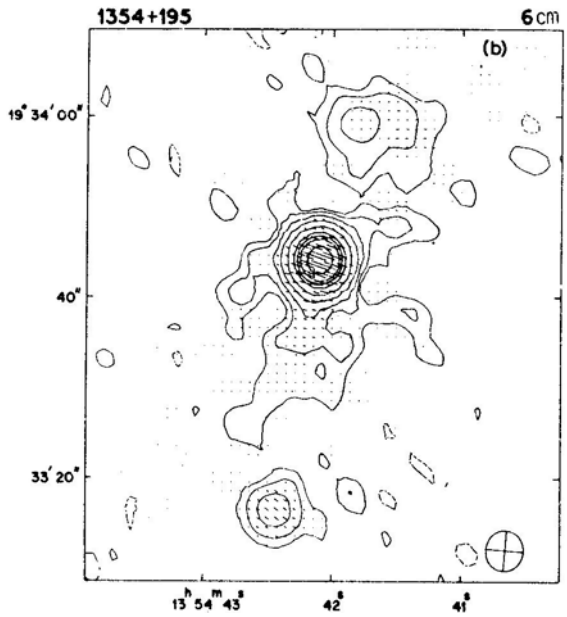

Figure 11. (b) 1354+ 195. Contours: 1202 × (–0.02, –0.01, 0.01, 0.02, 0.04, 0.08, 0.16, 0.30, 0.40, 0.50, 0.75).

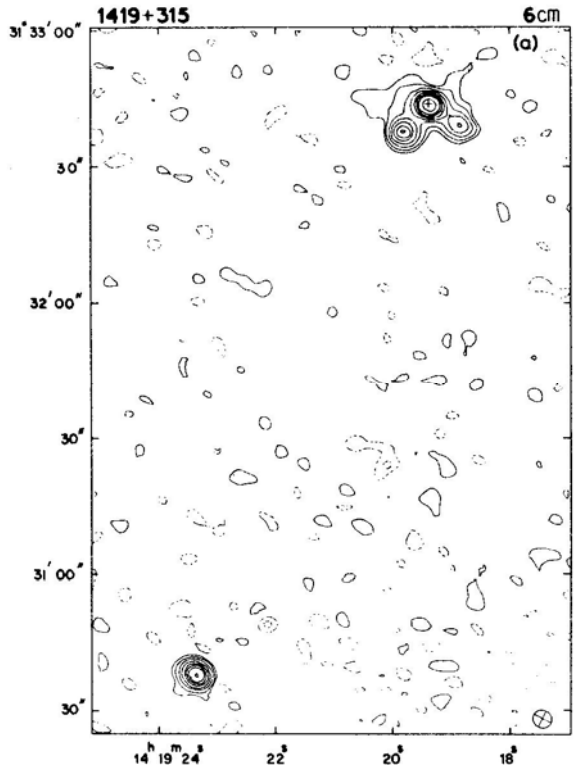

Figure 12. (a) 1419 + 315. Contours: 55 × (– 0.06, – 0.03, 0.03, 0.06, 0.12, 0.20, 0.30, 0.40, 0.50, 0.75).

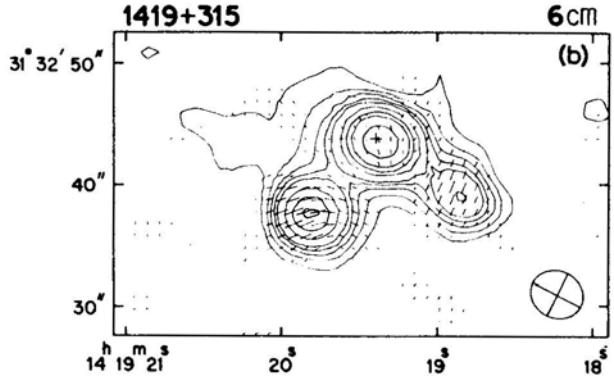

Figure 12. (b) 1419 + 315. Contours: 54 × (– 0.08, – 0.04, 0.04, 0.08, 0.12, 0.16, 0.20, 0.30, 0.40, 0.50, 0.75).

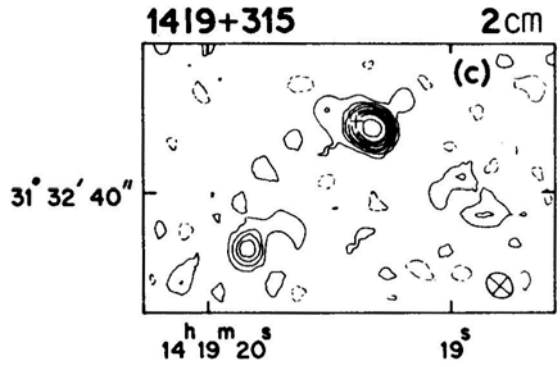

Figure 12. (c) 1419 + 315. Contours: 36 × (– 0.10, – 0.05, 0.05, 0.10, 0.15, 0.20, 0.30, 0.40, 0.50, 0.75).

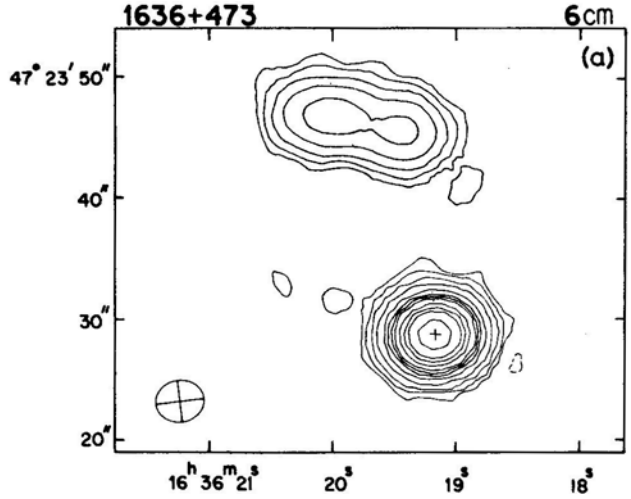

Figure 13. (a) 1636 + 473. Contours: 492 × (–0.01, –0.005, 0.005, 0.01, 0.02, 0.04, 0.08, 0.12, 0.16, 0.20, 0.30, 0.40, 0.50, 0.75).

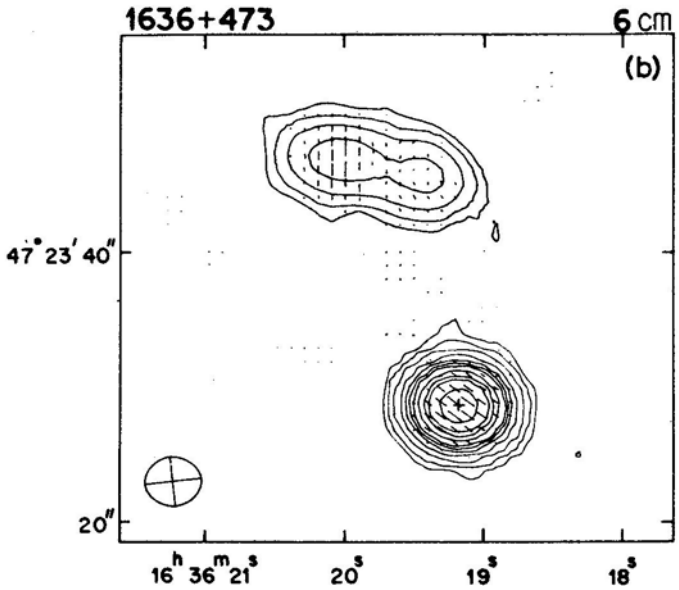

Figure 13. (b) 1636 + 473. Contours: 494 × (– 0.02, – 0.01, 0.01, 0.02, 0.04, 0.08, 0.12, 0.16 0.20, 0.30, 0.40, 0.50, 0.75).

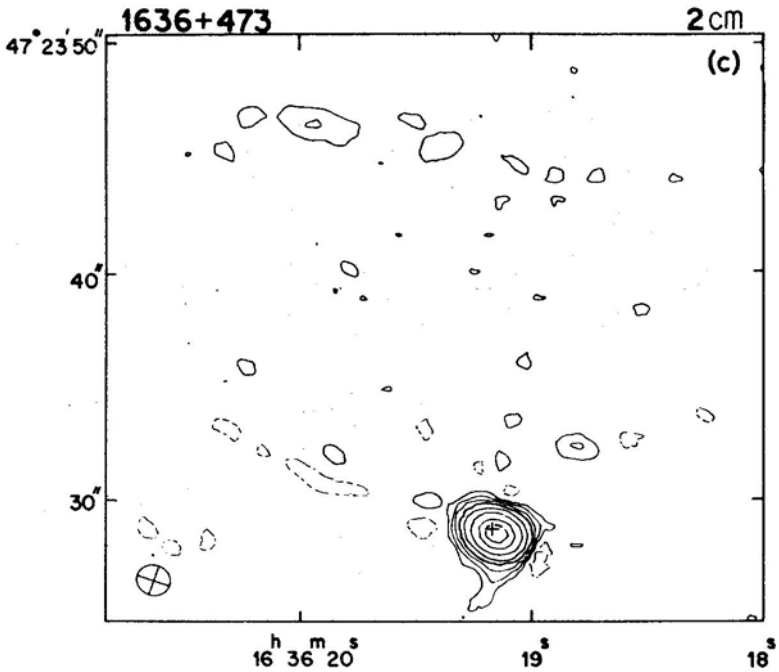

Figure 13. (c) 1636 + 473. Contours: 885 x (– 0.03, – 0.015, –0.0075, 0.0075, 0.015, 0.03, 0.06, 0.12, 0.25, 0.50, 0.75).

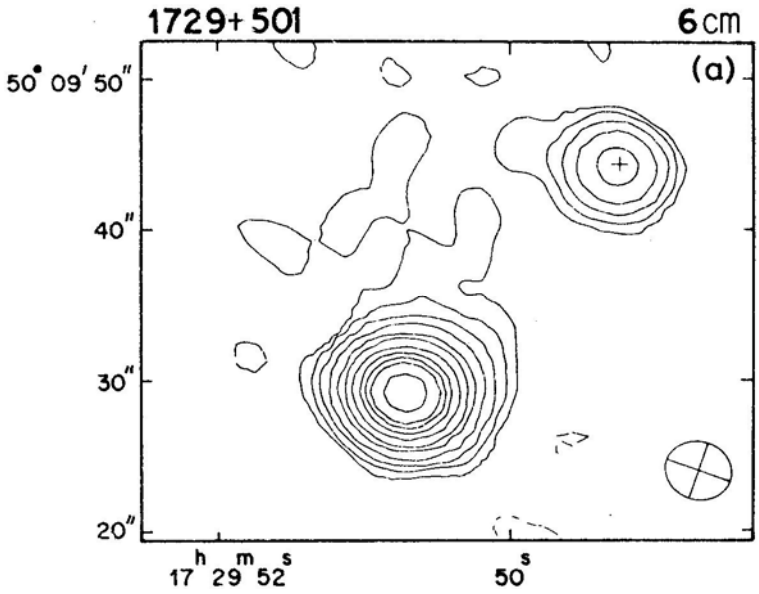

Figure 14. (a) 1729 + 501. Contours: 355 × (– 0.01, –0.005, 0.005, 0.01, 0.02, 0.04, 0.08, 0.12, 0.20, 0.30, 0.40, 0.50, 0.75).

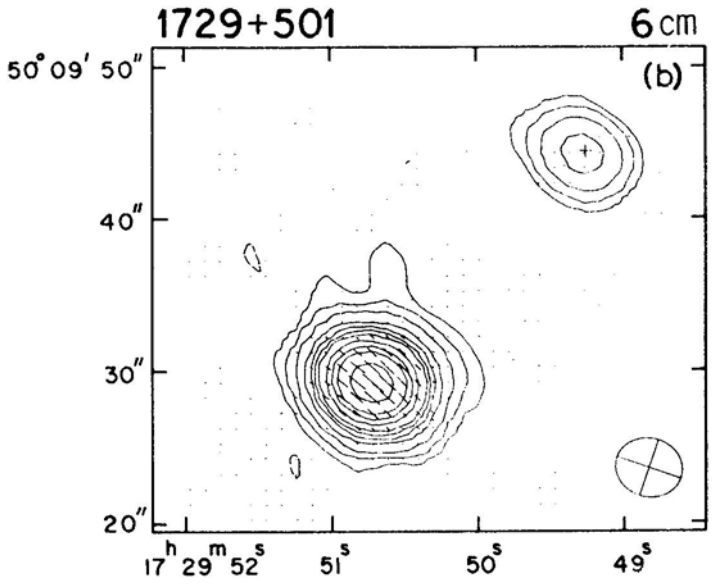

Figure 14. (b) 1729 + 501. Contours: 353 × (–0.02, – 0.01, 0.01, 0.02, 0.04, 0.08, 0.12, 0.16, 0.20, 0.30, 0.40, 0.50, 0.75).

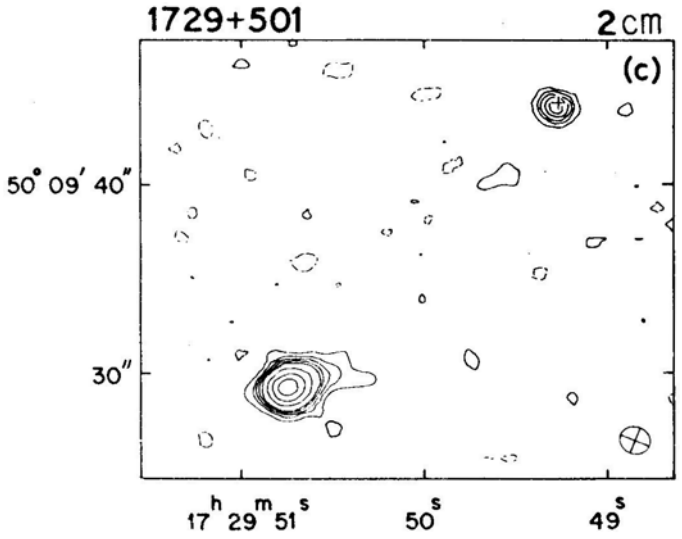

Figure 14. (c) 1729 + 501. Contours: 90 × (– 0.06, – 0.03, 0.03, 0.06, 0.09, 0.12, 0.16, 0.30, 0.50, 0.75).

Columns 3 and 4: The right ascension and declination (epoch 1950) of the sub-component. This gives the position of the best-fit, two-dimensional Gaussian, unless enclosed in parentheses, when it is the position of the pixel of maximum brightness. The pixels are separated by 1 arcsec at λ6 cm and by 0.4 arcsec at λ 2 cm.

Column 5: The deconvolved half-power width and orientation of the best-fit Gaussian to the sub-component. If the component width was less than half the HPBW in all directions it was considered to be unresolved and is marked u.

Column 6: The peak flux density (S_p) and the integrated flux density (S_1) of the sub-component in mJy. S_p is the height of the best-fit, two-dimensional Gaussian, unless enclosed in parentheses, when it is the intensity at the pixel of maximum brightness for weak and/or complex components. For S_1, the integrations were made over rectangular areas containing a complete component, or a combination of components, as indicated. All flux density values have been corrected for attenuation by the primary polar diagram.

Columns 7 to 9: These contain the information on the linear polarization characteristics of the component. In columns 7 and 8 the right ascension and declination of the pixel of maximum polarized intensity are given if significantly shifted from the position of the peak of the total power component. In such cases, the polarization percentage and PA (column 9) are also tabulated for the total power peak.

In Table 5b columns 1 to 6 are identical to that of Table 5a. Since at λ2 cm the pixel of maximum polarized intensity is coincident with the total power peak in all cases, the positions of peak polarization have not been included in the table. The polarization percentage and PA are listed in column 7.

For both λ6 and 2 cm, a correction for the effects of noise on the Stokes parameters Q and U was applied to the measured polarized intensity before computing the polarization percentage to give the most likely value of polarized intensity (Wardle &

Table 5a. λ6 cm data for the individual sources.

Source	Component	Right Ascension			Declination			Component size major	minor	PA	S_p	S_t	Right Ascension (polarization)			Declination (polarization)			Polarization per cent	PA (deg)
		h	m	s	°	′	″	(″)	(″)	(°)	(mJy)	(mJy)	h	m	s	°	′	″		
(1)	(2)		(3)			(4)			(5)		(6)			(7)			(8)			(9)	
0232−042	W	02	32	35.97	−04	15	09.4	u			184±11	184							10.8	30
	C			36.65			09.7	3.6	<2	70	226±17	285							⩽0.13	
	E												02	32	36.84	−04	15	08.7	⩾6.8	71
0309+411	C	03	09	44.82	41	08	48.9	u			337±17	337							2.2	30
0717+170	W	07	17	34.24	17	04	07.3	4.8	4.0	89	99±9	197							17.0	45
	C?			36.87			22.1	8.6	<2.0	65	4±0.5	9							⩽16.6	
	E			40.98			50.1	5.5	3.2	37	15±1	30							10.2	140
													07	17	41.09	17	04	49.3	19.7	132
0740+380	C	07	40	56.80	38	00	30.8	2.0	<2.0	142	213±11	229							0.6	24
	E1	(	41	00.03	37	59	05.4)				(8)	39								
	E2		41	00.39	37	58	59.8	2.6	<2.0	127	28±3								⩽0.8	
0742+376	W1	(07	42	18.69	37	39	14.7)				(44)	126	07	42	18.64	37	39	15.2	10.6	75
	W2	(		18.98		39	11.2)				(78)								3.9	143
	C			22.60		38	33.2	u			60±3	60							4.6	175
0821+394	C	08	21	37.34	39	26	28.1	u			1036±53	1247							1.4	120
0836+195	SW	08	36	14.75	19	32	07.1	6.3	3.9	161	3±0.4	7							⩽5.0	
	C			14.98			24.9	u			74±4	77							3.6	109
	NE			15.31			37.3	2.3	⩽2.2	2	68±4	88							7.7	95
0932+022	W	09	32	40.95	02	17	16.1	11.4	5.0	24	(51)	137	09	32	40.95	02	17	15.3	15.4	159
	C			43.00			41.2	6.3	2.4	53	(82)	143			42.93			40.6	1.1	125
	E	(		43.26			44.6)				(45)				43.26			44.1	5.7	115
1007+417	SW	10	07	25.91	41	47	05.6	3.2	2.3	111	302±16	454							8.8	160
	C			26.10			25.3	u			149±9	189							3.2	108
	NE			26.33			36.6	3.9	2.2	38	21±2	38							4.2	106

1047+096	W	10	47	45.11	09	42	12.3	5.2	<2.0	122	11±0.6	21											3.8	157
													10	47	45.23		09	42	11.7				8.6	16
	NW	10	47	48.59	09	42	1.6	4.9	3.6	1	5±0.5	13											9.0	48
													10	47	48.61		09	41	59.2				25.2	60
	C	(		49.02		41	44.7)				(29)				48.97				44.4				7.3	1
	SE			49.14		41	42.1	6.1	2.3	147	56±4	117			49.22				40.7				4.4	85
1055+201	NW	10	55	37.12	20	08	15.3	2.3	<2.0	94	510±27	690											3.2	125
													10	55	37.23		20	08	15.3				6.8	135
	C			37.55		07	54.9	u			846±43	959			36.95			08	15.3				3.9	90
															37.52			07	57.3				0.1	93
																							1.0	91
1320+299	C	13	20	40.52	29	57	23.8	u			277±14	298											4.7	135
	E1			42.21		57	12.3	2.1	<2.0	74	195±10	229											9.5	126
	E2			43.77		56	54.3	u			69±4	78											9.6	9
1347+539	C	13	47	42.61	53	56	08.5	u			836±43	891											1.8	13
1354+195	NW	13	54	41.73	19	33	59.2	5.3	3.7	65	60±5												3.4	178
													13	54	41.41		19	33	58.6				14.8	96
	C			42.10			44.1	u			1292±65	1761											4.8	70
	SE			42.43			16.6	2.0	≤2.0	119	73±5												14.3	50
1419+315	W	(14	19	18.82	31	32	38.8)				(17)												10.9	157
	C			19.36			43.5	3.5	2.3	86	54±5	140											1.6	13
	E	(		19.84			37.8)				(28)												11.6	108
	SE	14	19	23.37	31	30	38.1	u			54±3	54											≤0.9	
1636+473	C	16	36	19.17	47	23	28.8	u			500±25	500											1.6	53
	NE1	(		19.45			46.0)				48	150											1.5	164
	NE2	(		19.99			47.0)																11.8	179
1729+501	C	17	29	49.27	50	09	44.2	u			39±2	43											5.5	50
	E			50.71			29.3	1.6	<1.6	118	352±18	414											18.2	48

Table 5b. $\lambda 2$ cm data for the individual sources.

Source	Component	Right Ascension			Declination			Component size major	minor	PA	S_p	S_I	Polarization per cent	PA
		h	m	s	°	′	″	(″)	(″)	(deg)	(mJy)	(mJy)		(deg)
(1)	(2)		(3)			(4)			(5)		(6)		(7)	
0232−042	W	02	32	35.92	−04	15	09.7	1.2	0.7	166	33±3	75	⩽11.2	
	C			36.59			10.1				120±7	159	⩽ 2.9	
	E	(		36.80			09.4)				(12)		⩽23.1	
0309+411	C	03	09	44.78	41	08	48.8	u			465±39	465	2.1	39
0717+170	W	(07	17	34.24	17	04	07.5)				(12)	158	⩽20.9	
0740+380	C	07	40	56.78	38	00	31.0	1.9	0.75	136	30±2	78	⩽ 8.5	
	E2	(	41	00.42	37	58	59.9)				(⩽3.5)			
0742+376	W1	(07	42	18.46	37	39	15.8)				(8)	103	⩽38.2	
	W2	(		19.00		39	11.0)				(10)		⩽27.6	
	C			22.60		38	33.2	u			49±3	52	⩽ 6.4	
0821+394	C	08	21	37.31	39	26	28.2	u			992±54	1270	0.6	116
0836+195	C	08	36	14.97	19	32	25.0	0.7	⩽0.7	37	28±3	38	⩽ 5.7	
	NE			15.30			37.8	1.3	⩽0.7	75	11±1	18	⩽21.9	
0932+022	C	09	32	42.94	02	17	41.1	u			76±4	93	⩽ 3.9	
	E	(		43.30			44.8)				(11)	25	⩽22.2	

1007+417	SW	10	07	26.00	41	47	05.2				(52)	183	⩽ 9.9	
	C			26.11			25.3	u			70±5	111	⩽ 4.8	
	NE			26.28			37.0				7±1	20		
1047+096	C	10	47	48.92	09	41	47.0	1.2	0.7	122	16±2	112	⩽27.5	
	SE			49.15			41.1	3.8	0.8	51	7±2		⩽22.4	
1055+201	NW	10	55	37.16	20	08	15.7	1.7	0.9	87	103±11	277	⩽ 2.8	
	C			37.56		07	55.3	u			832±53	889	5.4	175
1320+299	C	13	20	40.51	29	57	23.6	u			159±9	159	4.3	149
	E1			42.17		57	12.0	0.75	<0.70	70	39±4	49	16.9	133
	E2			43.75		56	54.1	1.6	<0.70	36	14±3	29	⩽24.7	
1347+539	C	13	47	42.58	53	56	08.4	u			611±32	666	4.5	50
1354+195	C	13	54	42.07	19	33	43.9	u			944±48	1048	3.4	55
1419+315	W	(14	19	18.86	31	32	38.8)				(4)			
	C			19.33			43.4	u			38±3	89	⩽ 7.4	
	E			19.83			37.1	1.35	<0.7	155	9±2			
1636+473	C	16	36	19.15	47	23	28.5	u			914±47		1.3	53
	NE1			19.34			45.6				(13)	991		
	NE2			19.89			46.4				(13)			
1729+501	C	17	29	49.28	50	09	44.1	u			18±2	23	⩽10.7	
	E			50.74			29.3	1.2	0.6	120	93±6	142	10.2	43

Kronberg 1974). When upper limits on the polarization percentage are given these represent a lσ polarized intensity.

4. Spectra

The integrated spectra of the 17 sources and, where possible, the spectra of individual components are shown in Fig. 15. All the total flux densities are on the scale of Baars *et al.* (1977) and have been compiled largely from the catalogues listed by Kühr *et al.* (1979, 1981). Estimates of the total flux density from aperture synthesis observations have sometimes been included, usually either to extend the spectrum to higher frequencies or to provide information at frequencies for which single-dish measurements are not available. These flux densities have been estimated either from the correlated flux density at the shortest spacings or from a sum of the component flux densities. Wherever possible, the component flux densities have also been converted to the scale of Baars *et al.* (1977). We have assumed an error of 10 per cent in the flux density, unless the quoted error is larger than this value.

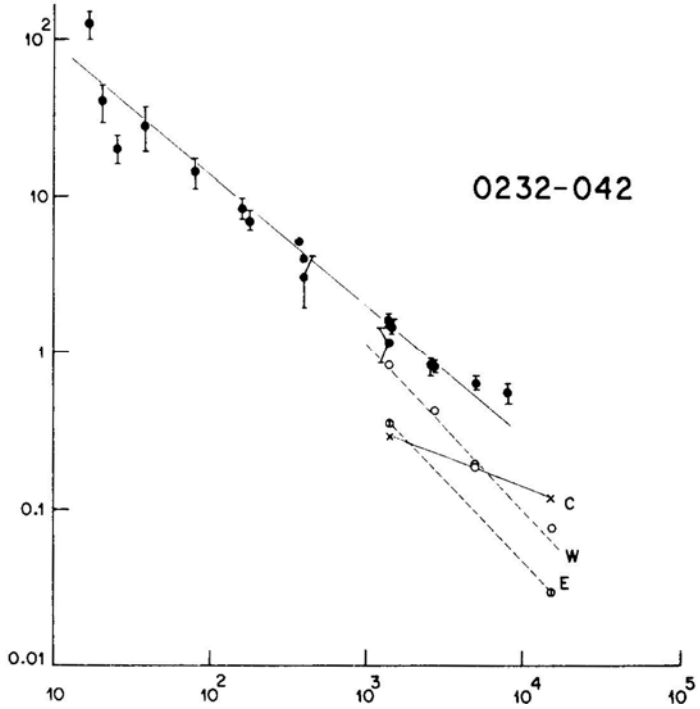

Figure 15. The spectra of the entire source and the individual radio components. The frequency values are in MHz while the flux densities are in Jy. The filled circles represent the total flux density measurements, and the solid curves, the best fits to these points. The spectra of the individual components are shown by broken lines. The different components are represented by the following symbols. × : core (C); : western (W), south-western (SW) and north-western (NW); ⊕ : eastern (E), north-eastern (NE) and the northern triple source in 1419 + 315; ⊗: the western component of 1047 + 096; Θ : the triple source of 1047 + 096, the southern component of 1419 + 315 and the far-eastern component (E2) of 1320 + 299.

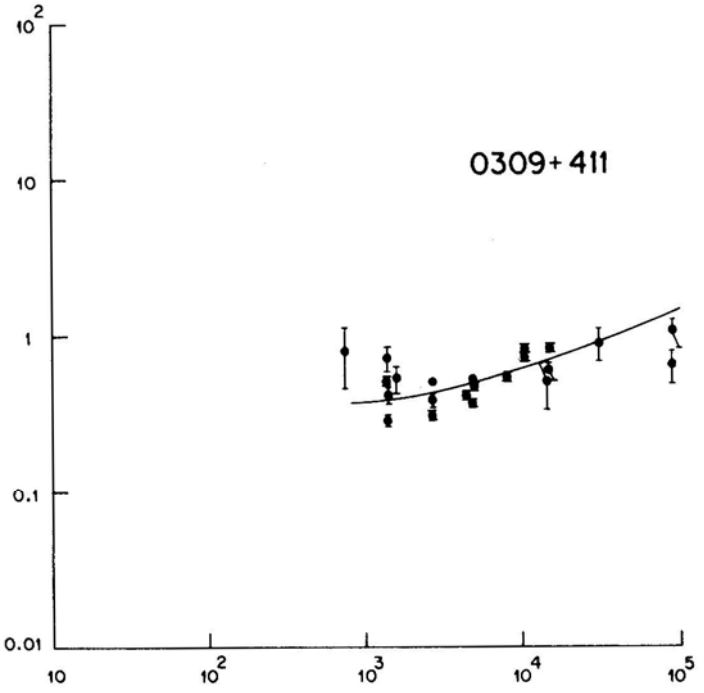

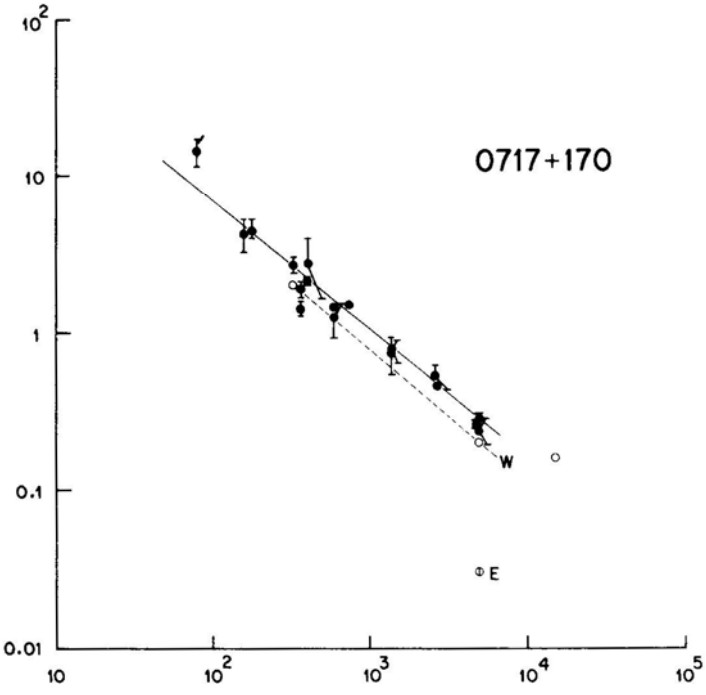

Figure 15. Continued

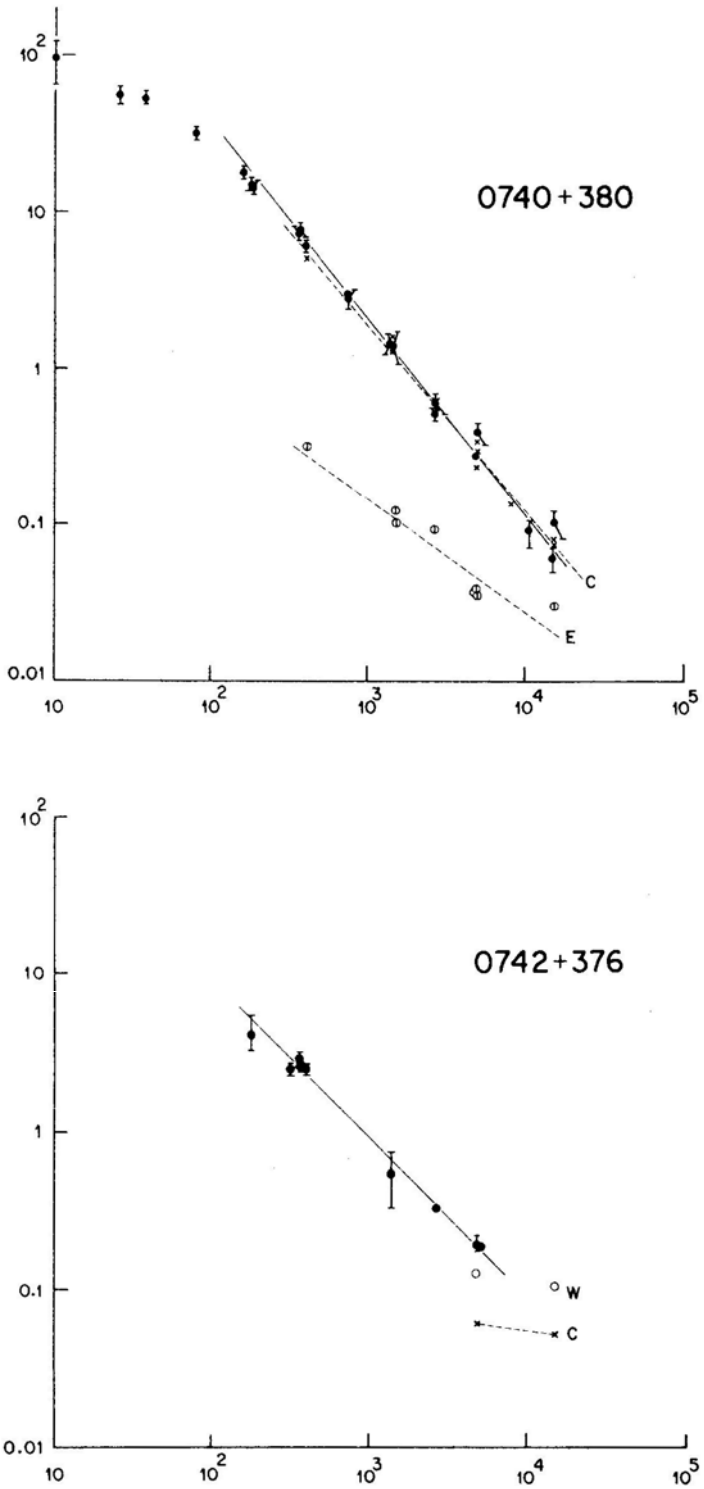

Figure 15.

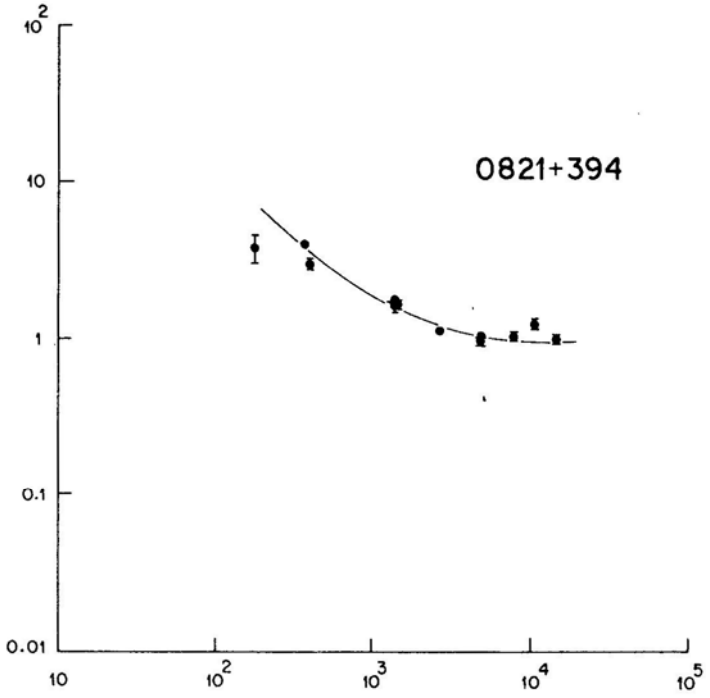

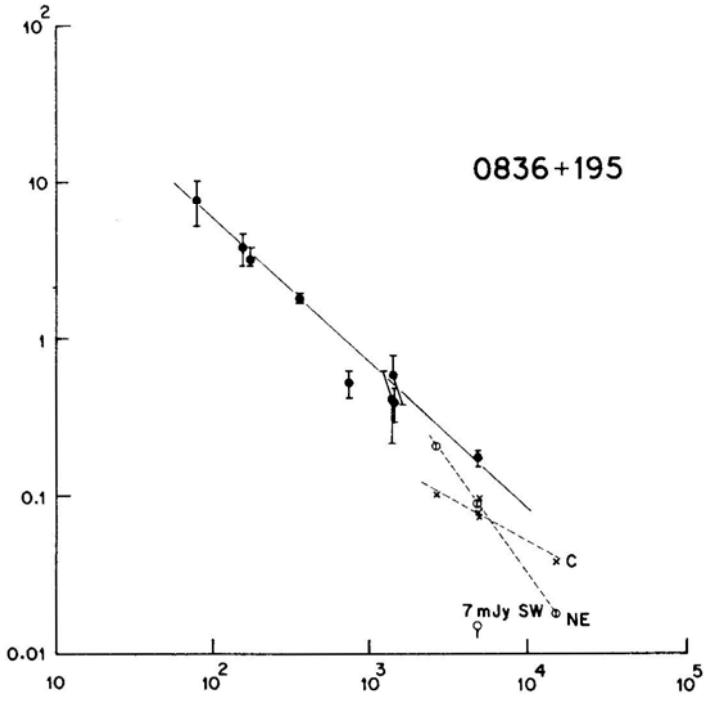

Figure 15. Continued.

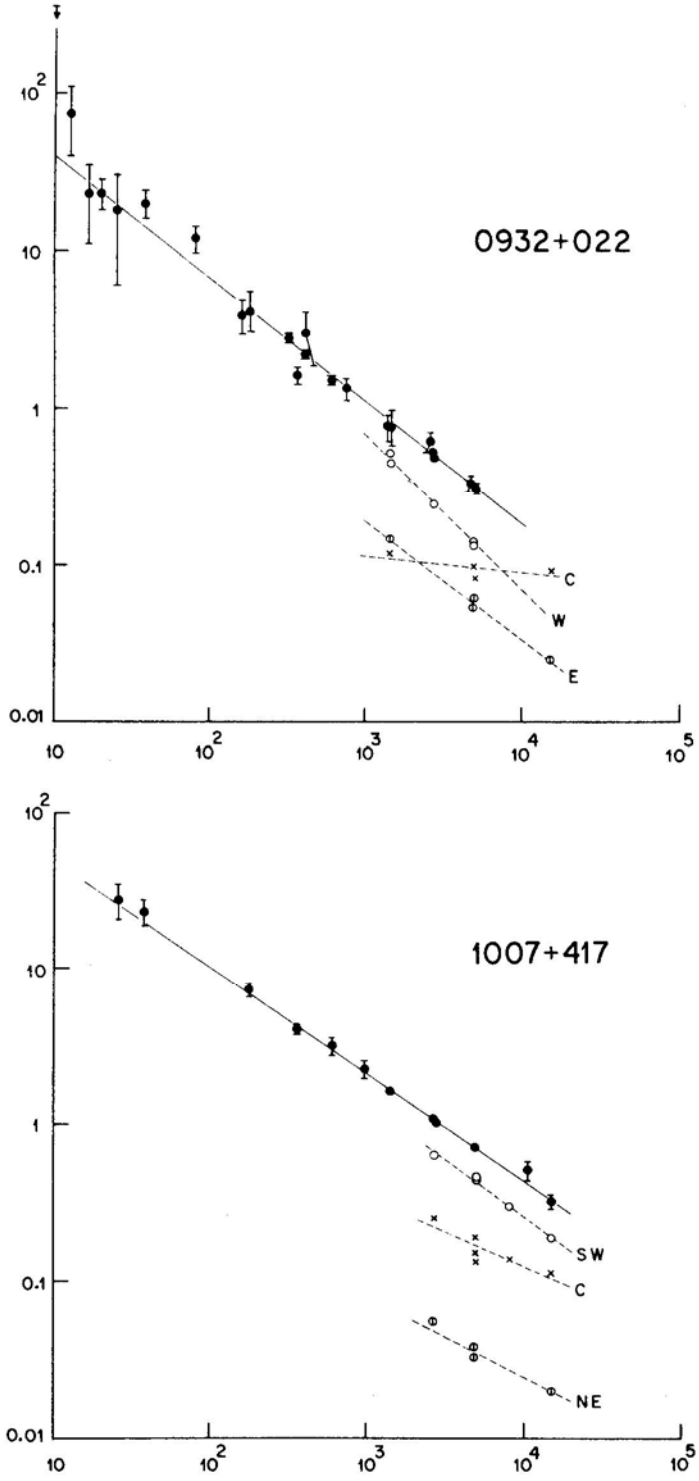

Figure 15. Continued.

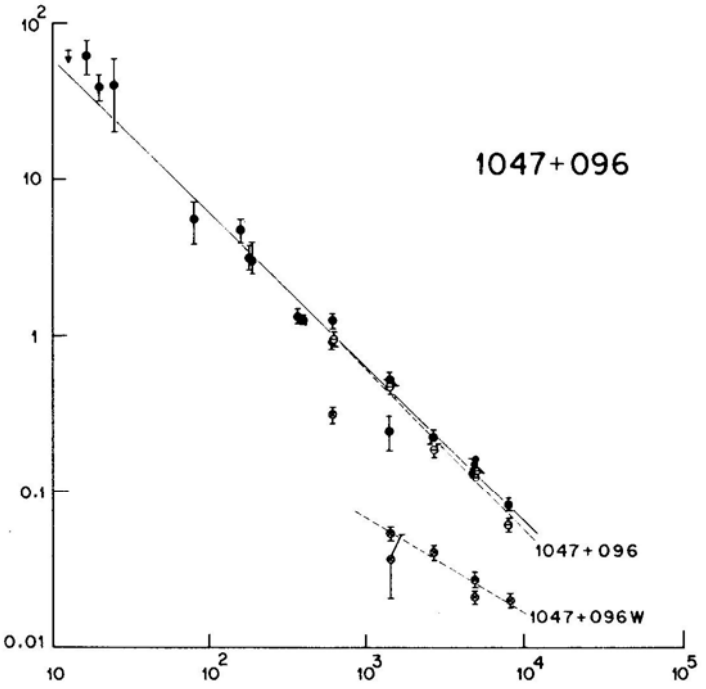

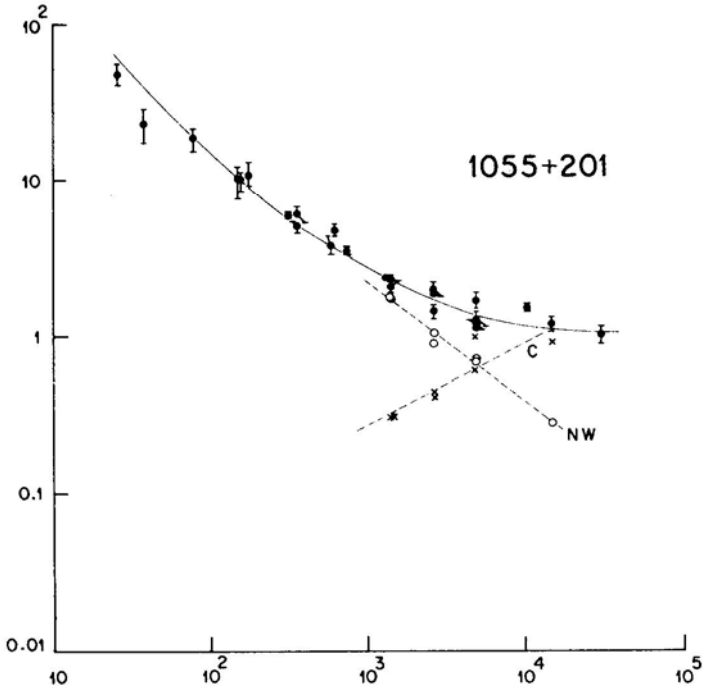

Figure 15. Continued.

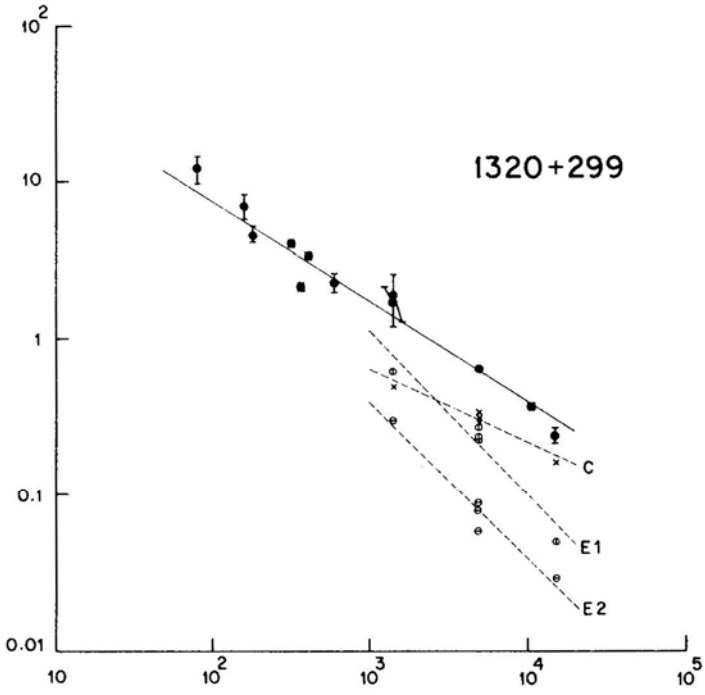

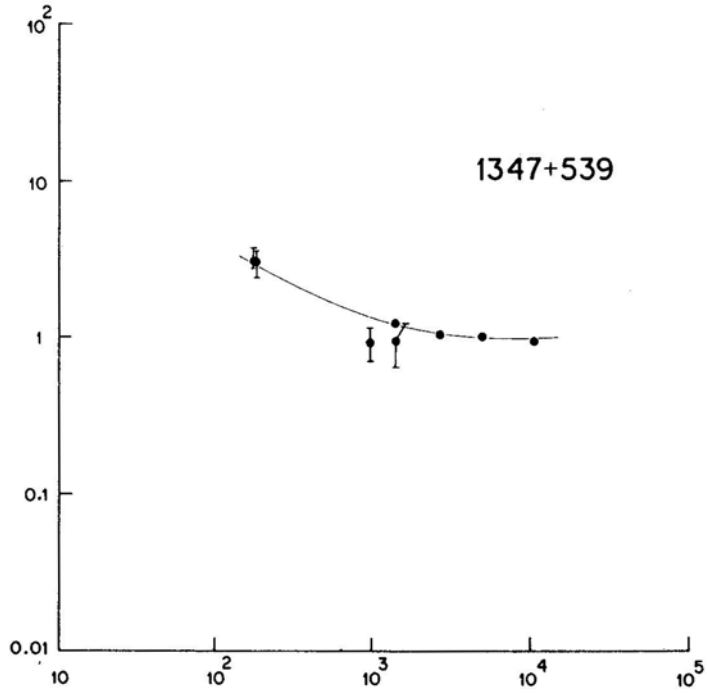

Figure 15. Continued

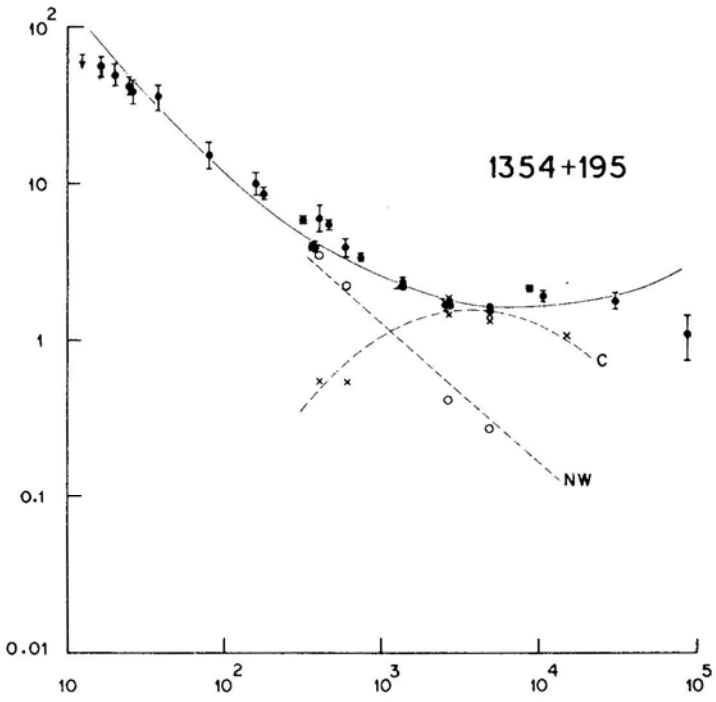

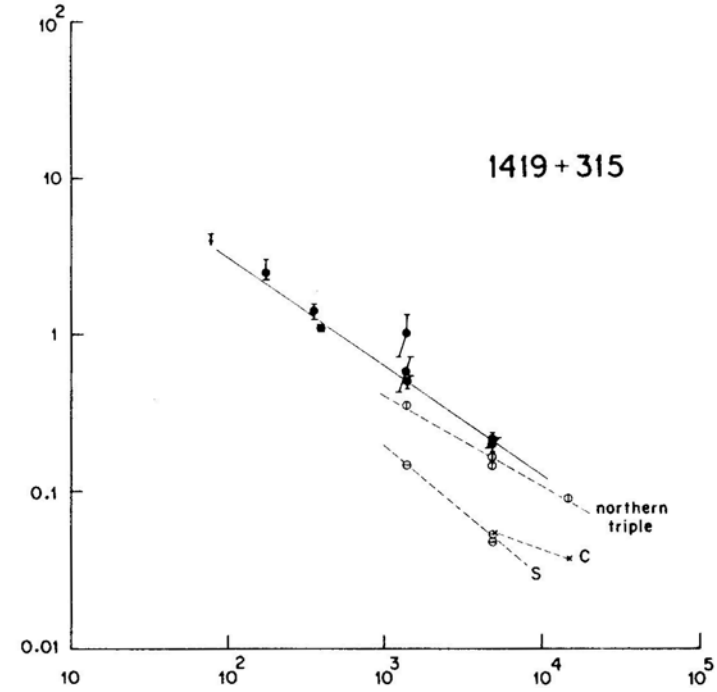

Figure 15. Continued.

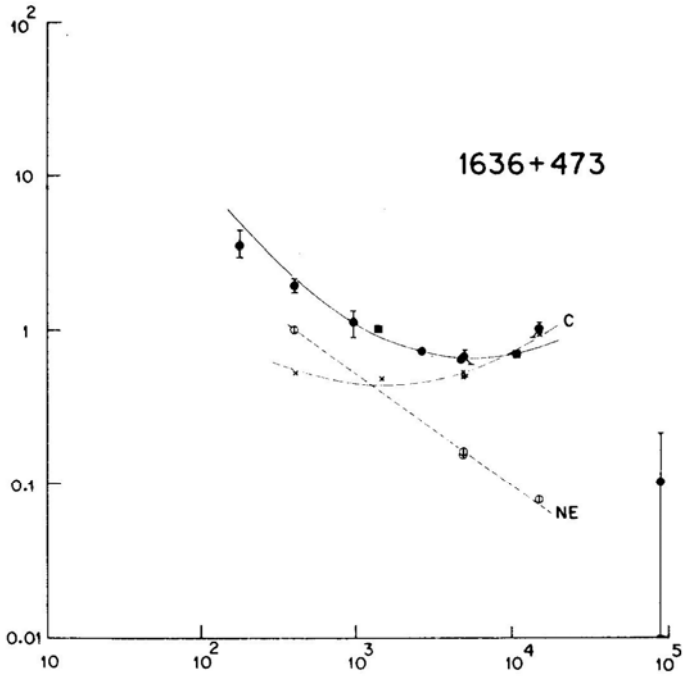

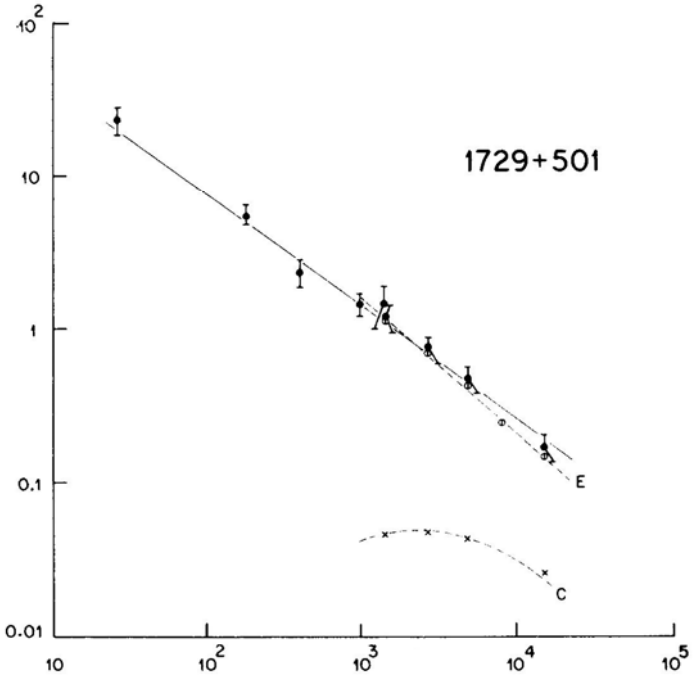

Figure 15. Continued.

A linear fit has been made to the spectrum unless it appears significantly curved, in which case we have fitted a spectrum of the form $\log S = a + b \log \nu + c \log \nu^2$. Both the linear and parabolic least-square fits were made using the NOD2 package (Haslam 1974) at Bangalore.

5. Notes on individual sources

023–2042

This is an asymmetric source where the $\lambda 2$ cm flux-density ratio of the OCs is ~ 2, and the ratio of their separations from the core is ~ 3. The eastern component is ~ 3 arcsec from the core and hence was not separated from it by MH 78. We find no evidence for the component they suggested 28 arcsec to the west. Hintzen, Ulvestad & Owen (1983, hereinafter HUO) have found a jet/bridge connecting the western component to the core at $\lambda 20$ cm.

The integrated spectrum of the source is straight below ~ 2 GHz with a spectral index ($S \propto \nu^{-\alpha}$) $\alpha = 0.83 \pm 0.06$, and appears to flatten at higher frequencies. The spectral indices of the individual components are $\alpha_W = 1.05 \pm 0.08$, $\alpha_E \simeq 1.0 \pm 0.1$ and $\alpha_C = 0.38 \pm 0.06$.

The rotation measure (RM) has been reported to be 4.6 ± 1.2 rad m^{-2} with the intrinsic E vector in PA $34 \pm 3°$ by Tabara & Inoue (1980, hereinafter TI80) and 5 ± 1 rad m^{-2} at $32 \pm 3°$ by Simard-Normandin, Kronberg & Button (1981, hereinafter SKB 81). The 5 GHz polarization integrated over the source gives a PA consistent with the above values although the PAs for the eastern and western components differ by ~ 40°. The central component is. unpolarized.

0309 + 411

Kapahi (1979) reported this source to have an unresolved core coincident with an 18-mag galaxy and an extended component ~ 87 arcsec to the north-west with a flux density of ~ 150 mJy at 1415 MHz. Only the core component was detected in our observations. If the extended component, which we estimate from Kapahi's observation to have a size ~ 40 arcsec × $\lesssim$ 40 arcsec, were to possess $\lesssim 3\sigma$ brightness, then its flux density at $\lambda 6$ cm would be $\lesssim$ 250 mJy. Recently, we have observed this source with the VLA at 1415 MHz with a beam size of about 6 × 4 arcsec but did not detect the outer component implying an upper limit of ~ 160 mJy at 1415 MHz. Although this could be just consistent with Kapahi's observations, we do not find any emission at the peak position of the extended component to a level of ~ 2.5 mJy/beam at 1415 MHz. A VLA D-array $\lambda 20$ cm map would be useful to investigate the extended structure.

For $\nu \gtrsim 2$ GHz, the continuum spectrum appears to rise slowly. Observations are clearly required to study the spectrum at frequencies $\lesssim 1$ GHz. A large spread is apparent in the measured flux densities at 1.4, 2.7, 5 and 15 GHz implying that the core is strongly variable.

The polarization percentages are similar at $\lambda 6$ and 2 cm and the measured position angles imply a RM of about -50 ± 25 rad m^{-2}. However, our position angles seem incompatible with the value of $83 \pm 8°$ measured by Simard-Normandin, Kronberg & Button (1982) at 10.5 GHz, although their percentage polarization (1.3 ± 0.4) is in reasonable agreement with our values. Earlier, Simard-Normandin, Kronberg &

Neidhöfer (1981) had reported a polarization percentage of 6.55 ±0.6 at PA= 13 ±2° at 1600 MHz. It seems very likely that the source is also a polarization variable and further measurements would clearly be of interest.

0717+170

This source was not included in the list of one-sided sources of K 81. It was discussed by Joshi (1981), who suggested a possible head-tail structure for the source. From occultation scans at 327 MHz, Joshi concluded that the source consists of a 'head' containing ~ 75 per cent of the total flux density and a 'tail' of length ~ 100 arcsec at PA~ 71° with a weak secondary component at the end of the tail. He found an18-mag red galaxy close to the 'head' of the source and suggested it as a possible identification.

The present observations at l 6cm give a source size of 106 arcsec in PA 66°. However, the morphology of the source looks very similar to a high-luminosity class II source of Fanaroff & Riley (1974), with a possible weak central component which appears extended along the source axis at λ6 cm. The polarization information also suggests that he two outer components represent the lobes of at typical double source. Additional evidence for the western component being a lobe of a double source comes from the λ2 cm map. An extremely relaxed structure is seen with no evidence of any strong compact component coincident with the 18-mag galaxy marked in Fig. 3.

A search near the central component revealed no new candidate optical identification above the limit of the Palomar Observatory Sky Survey (POSS) prints. However, there are several other galaxies in the field (marked on Fig. 3). It seems likely from the above arguments that the proposed identification of Joshi (1981) is a chance superposition. We presently classify this source as unidentified.

The radio source has a straight spectrumbetween80 MHz and 5 GHz with α =0.81 ± 0.04.The two-point spectral index of the western component is 0.85 ± 0.05 between 327 and 4885 MHz. The apparent excess flux density from the western component at 15 GHz may not be significant in view of the low surface brightness of the source at this frequency.

0740 +380.

The source consists of two components separated by ~ 100 arcsec. The stronger is coincident with a 17.6-mag quasar. Whether the two components are physically related is not clear. There is no bridge connecting them but also no optical object is visible on the POSS prints at the position of the SE component.

The core component was found to be a close double of separation 1.8 arcsec at PA 131.5° by Wilkinson, Richards & Bowden (1974). The double structure has been confirmed by Schilizzi, Kapahi & Neff (1982) who report a separation of 1.2 arcsec along PA 137°. The accurate quasar position measured by Clements (1983) is—within the errors—equidistant from the two peaks in the core component.

The integrated radio spectrum appears straight above 100 MHz with α = 1.24 ± 0.02, but appears to flatten below this frequency. The spectral index of the core (~ 1.19 ± 0.04). is similar to the integrated source spectrum. However, the spectrum of the SE component is substantially flatter with a spectral index of 0.71 ± 0.09. VLBI observations of the core at 1417 MHz with a baseline of 1.26 Mλ showed a maximum correlated flux density of ~ 22 per cent of the total flux density at this frequency

(Kapahi & Schilizzi 1979). As noted by these authors, this is unlikely to be due to any flat-spectrum nuclear component.

Using only the measurements > 2σ among those quoted by TI80 and our VLA observations gives a RM ~ 30 rad m^{-2} and an intrinsic PA ~ 15°.

0742 + 376

This source appears to be one-sided with an angular size of ~ 62 arcsec, consistent with the structure reported by Katgert-Merkelijn, Lari & Padrielli (1980). The integrated spectrum is straight between ~ 150 MHz and 5 GHz, with α = 1.00 ± 0.02. The two-point spectral index for the core is about 0.1 ± 0.1 between 5 and 15 GHz. The 15-GHz flux density of the western component is unreliable due to its low brightness. An intriguing aspect of this source is the change in PA of the l6 cm polarization by ~ 70° between components W1 and W2.

0821 + 394

A secondary radio component south-west of the core was reported by Stannard & Neal (1977) and Kapahi (1981b). However, the positions given by these authors differ by ~ 16 arcsec. Stannard & Neal (1977) have also noted that the structure is uncertain due to the presence of a confusing source ~ 6.2 arcmin away along PA 60° (*cf.* Bridle *et al.* 1972). Potash & Wardle (1979) observed this source at 2.7 and 8.1 GHz and did not detect the secondary component, setting an upper limit of 50mJy for it at both frequencies.

We find no evidence for this component in our data and suggest that it is unreal. It appeared barely resolved by Kapahi (1981b) at λ6 cm who found its flux density to be ~ 130 mJy. With our beam of 4.6 ×4.3 arcsec at λ6 cm and a root-mean-square (rms) noise of ~ 6.4 mJy/beam we should have certainly detected this component, if real. It is curious, however, that the spectrum appears to steepen at low frequencies, suggesting that there is extended emission.

The RM is 14 ± 5 rad m^{-2} with an intrinsic PA of 119 ± 7° (SKB 81). Our measured PAs of 116° and 120° at λ*2* cm and λ6 cm respectively are similar to the intrinsic value.

0836 + 195

This is a triple source with a prominent core and a flux-density ratio of ~ 13:1 at λ6 cm for the outer components. The SW component flux density of 7 mJy is consistent with the < 10 mJy limit of MH 78. It is also lower than the noise level of Jenkins, Pooley & Riley (1977). The SW component has possibly been detected by Douglas *et al* (1980) at 365 MHz who deduced the source size to be 28 ± 1 arcsec along PA 9 ± 3°, in broad agreement with our value of ~ 31 arcsec along PA ~ 15°. The integrated spectrum of the source is straight between 80 MHz and 5 GHz with α = 0.92 ± 0.05. The spectral index of the NE component appears to be rather high (~ 1.4) but more accurate flux densities are required to check this. For the core we find α = 0.58 ± 0.07 between 2.7 and 15 GHz.

The RM of the source is 10 ± 1 rad m^{-2} with an intrinsic PA of 98 ± 4° (SKB 81) which is consistent with our observations at λ6 cm.

0932 + 022

The outer components are very asymmetrically located with a separation ratio of ~ 8. The eastern component is at a distance of ~ 5 arcsec from the core along PA ~ 45°, and was not resolved from the core by MH 78. On the western side of the core, there is a weak component at ~ 3.5 arcsec from the core with $\alpha \simeq 1$ and S_{1413} ~ 9 mJy, in addition to the normal edge-brightened lobe at ~ 40 arcsec from the core (HUO; Swarup, Sinha & Hilldrup 1984). This component has not been resolved from the core in our λ6 cm map and is too weak to be detected in the λ2 cm observations.

The spectral index of the entire source is 0.78 ± 0.02 while those of the western and eastern lobes are 0.99 ± 0.05 and 0.76 ± 0.03 respectively. The core spectral index is 0.11 ±0.09 between 1.4 and 15 GHz. From long-baseline interferometric observations at Jodrell Bank, Bentley *et al* (1976) detected a flux density of 150 ± 50 mJy at 1666 MHz from a component with size < 0.1 arcsec. Since both the outer hot-spots appear to be resolved by the VIA with a 0.5 × 0.5 arcsec beam at λ6 cm (Swarup, Sinha & Hilldrup 1984), the compact component seen by Bentley *et al.* (1976) is possibly the core. Within their quoted errors, their 1666-MHz flux density is consistent with the core spectrum.

The RM of this sourceis –11± 1 rad m^{-2} with an intrinsic PA = 157 ± 5° (SKB 81). This is consistent with our values at λ6 cm. The most polarized feature on our map is the SW component which is ~ 15 per cent polarized along PA ~ 159°.

1007 + 417

This source was not in the K 81 list of one-sided sources. It was included in these observations because of the high flux-density ratio for the outer components reported by Owen, Porcas & Neff (1978). The northern component has a λ6 cm flux density of ~ 38 mJy, implying a flux density ratio of ~ 12.

The source has a straight spectrum with α = 0.68 ± 0.01 between 20 MHz and 15 GHz. The spectral indices of the northern and southern lobes are 0.51 ± 0.10 and 0.72 ± 0.04 respectively. The core spectral index is 0.44 ± 0.13. This appears to be steeper than the true spectrum of the core due to the presence of a jet which has been recently mapped by Owen & Puschell (1984) and by Saikia, Kulkarni & Porcas (in preparation).

1047 + 096

This source was suspected to be one-sided from the observations of MH 78. They suggested that the extreme western component, W, ~ 60 arcsec from the central source is related to it and the eastern component, if any, is below the detection limit, implying a flux-density ratio $\gtrsim$6 at λ6 cm. From the present VLA observations we find the central component of MH78 to be itself a triple with LAS ~ 21 arcsec. This source was also observed at the VLA at 1413 MHz by HUO who did not detect the northern lobe of our triple. We find this northern component to have a total flux density of ~ 13 mJy at λ6 cm and a size of 4.9 × 3.6 arcsec along PA 1°, consistent with its non-detection by HUO to a limit of ~ 4 mJy/beam at 1413 MHz.

MH 78 suggested a possible jet linking the central source to the extreme western component, W. There appears to be no evidence of such a jet in either our data or those of HUO. In the map of HUO, the component W itself seems to be a double source. We

have looked for a possible optical identification of this component but find no object above the limit of the POSS prints. Presently, we suggest that this is an unrelated background source.

The spectrum of the entire complex appears straight between ~ 16 MHz and 8 GHz ($\alpha \sim 0.98 \pm 0.03$). The spectral index of the western, possibly unrelated, source is 0.60 ± 0.10 between 1.4 and 8 GHz, while that of the triple associated with the quasar is 1.02 ± 0.07 between ~ 0.6 and 8 GHz. The 610-MHz flux density of the western source appears to be overestimated and has not been used in evaluating the spectral index.

Reliable measurements of the integrated polarization are not available to determine the rotation measure.

1055 + 201

This source appears to have a one-sided radio structure. HUO have observed it at 1413 MHz and also find it to be one-sided with LAS ~ 21 arcsec. The only suggestion of extended structure on the opposite side of the core is from the observations of Douglas *et al.* (1980) at 365 MHz who find the source to be an asymmetric double with a flux-density ratio of ~ 8.5 and LAS ~ 50 arcsec, but their PA of –78 ± 2° for their model fit is not consistent with our data.

The integrated spectrum of the source is straight below ~ 1 GHz ($\alpha = 0.69 \pm 0.02$) but tends to flatten at higher frequencies. The spectral index of the extended component is 0.76 ± 0.04 between 1.4 and 15 GHz. The core has an inverted spectrum ($\alpha = -0.52 \pm 0.12$) between 1.4 and 15 GHz. Our measured flux density of the core at 5 GHz is higher than that of MH 78 at the same frequency by ~ 60 per cent suggesting that the core may be variable.

The source has a RM of –22.8 ± 2.2 rad m^{-2} and an intrinsic PA of 123 ± 5° (TI80). Our λ6 cm PAs are consistent with this value.

1320 + 299

This source has an interesting asymmetrical structure with two outer components on the same side of the nucleus and an overall angular extent of ~ 51 arcsec. It has been discussed recently in some detail by Feretti, Giovannini & Parma (1982). Further VLA observations and a more detailed discussion will be presented elsewhere (Cornwell *et al,* in preparation).

The integrated spectral index of the source is 0.64 ± 0.03 between ~ 80 MHz. and 15 GHz. The spectral indices for the core and the components E1 and E2 are 0.46 ± 0.07, 1.04 ± 0.16 and 0.99 ± 0.12 respectively. The outer components appear to have similar spectral indices. However, the spectrum of El appears to steepen above ~ 5 GHz, with $\alpha_{1.4}^{5} = 0.73 \pm 0.07$ and $\alpha_{5}^{15} = 1.43 \pm 0.09$. Further observations at 15 GHz are needed to verify this steepening in the spectrum.

By combining our measurements with those of Feretti, Giovannini & Parma (1982), we estimate the RM for the nucleus and component E2 to be ~ 2 ± 3 and ~ 3 ± 0.3 rad m^{-2} respectively, the intrinsic PAs being ~ 150° and ~ 10° respectively. The RM of E1 is also small with an intrinsic PA ~ 130°, but has larger uncertainties because of the smaller range in wavelength for which polarization data are available.

1347 + 539

This source was suspected to have one-sided radio structure from the observations of Owen, Porcas & Neff (1978) who detected a marginally resolved component with a flux density of 50 ± 18 mJy at 2695 MHz at a distance of ~ 31 arcsec from the core. We do not detect this component in the present observations with a beam of ~ 4.9 × 3.8 arcsec and an rms noise of ~ 1.8 mJy/beam at λ6cm. Recent VLA observations with the A array at λ6 cm (Perley 1982; Owen & Puschell 1984) show one-sided emission extending upto ~ 5 arcsec to the NW of the core.

1354 + 195

This is a core-dominated triple source with an extent of ~ 44 arcsec, and a possible jet towards the southern component. The outer components are of similar intensity but are asymmetrically located with respect to the core. The separation ratio is 1.76. The SE component was not detected by MH78 and Macdonald & Miley (1971), but has recently been mapped at Cambridge by Peacock & Wall (1982). The radio spectrum is straight below 2 GHz (α = 0.65 ± 0.04) but flattens above this frequency. Assuming that the weaker component detected by Wilkinson, Richards & Bowden (1974) is the core, then the core spectrum turns over around 1–2GHz.The spectral index of the NW component is 1.04 ± 0.05.

Marscher & Broderick (1983) have made VLBI observations of this source and find structure on scales ranging from a fraction of a milliarcsec to ~ 7 milliarcsec. The most compact structure consists of an equal double separated by ~ 0.75 milliarcsec along PA –29°, close to the PA of the entire source.

The RMs suggested for this source are 4.2 ± 0.8 rad m^{-2} with intrinsic PA 72 ±1° (TI80) and 5 ± 1 rad m^{-2} with PA 69 ± 2° (SKB 81). Our λ6 cm PAs are consistent with these values.

1419 + 315

This source was suggested to be one-sided by Fanti *et al.* (1977) and Fanti *et al.* (1979a). While the core component appeared resolved in their observations the outer component located ~ 130 arcsec to the south-east appeared unresolved. In the present observations the outer component still appears unresolved at λ6 cm but the core is resolved into three components misaligned by about 80°. The quasar is co-incident with the middle component which is also the most weakly polarized of the triple and has a flat spectrum (α ~ 0.31 ± 0.11). The magnetic field lines appear to follow the bends in the overall structure.

The spectral index of the northern triple is 0.58 ± 0.07 between 1.4 and 15 GHz while that of the distant southern component is 0.84 ± 0.09 between 1.4 and 5 GHz. The spectrum of the entire complex appears straight between 178 and 5000 MHz with $\alpha \sim 0.69 \pm 0.04$.

The southern component could be an independent source unrelated to the triple structure. An examination of the POSS prints, however, showed no possible identification for this component.

1636 + 473

The extended emission is inclined at ~ 70° to the line joining the core to the nearest peak in the extended structure. The source has been observed with better resolution with MERLIN (Browne *et al.* 1982; Wilkinson 1982).

The extended component appears somewhat similar to a normal double radio source. We have looked for a possible identification for this on the POSS prints but find no likely candidates. It is of interest that from VLBI observations, Porcas (personal communication) finds the core to be extended by ~ 0.5 milliarcsec in the north-south direction.

The integrated spectrum of the source flattens at high frequencies and possibly rises above ~ 10 GHz. Although the 90 GHz measurement has large errors it shows that the spectrum must steepen again between 10 and 90 GHz. While the spectrum of the core appears to be curved, that of the extended emission is straight between 408 MHz and 15 GHz with $\alpha \sim 0.72 \pm 0.03$.

The PAs of polarization vectors in the core are similar at λ6 and 2 cm. Assuming Faraday rotation to be small at λ6 cm, the magnetic field of the extended component appears to be along its axis.

1729+501

This source appears to be one-sided but has a relatively weak core contributing only ~ 10 per cent of the total flux density at λ6 cm. HUO also find the source to be one sided from λ20 cm VLA observations.

The core spectrum appears to flatten below ~ 5 GHz. The integrated spectrum appears straight between 26 MHz and 15 GHz with $\alpha \sim 0.73 \pm 0.03$. The 26-MHz flux density has been estimated by subtracting the extrapolated flux density of the confusing source, 4C49.29, at this frequency. The spectral index of the extended component to the east is 0.87 ± 0.03 between 1.4 and 15 GHz.

6. Conclusions

Of the 17 sources observed, five appear one-sided on the present maps, three are unresolved while seven have radio lobes on both sides of the nucleus. Of the remaining two sources, 0717 + 170 is a double-lobed source whose identification is probably incorrect, while for 0740 + 380, the association of the outer component with the core is uncertain. Higher resolution observations of one of our unresolved sources, namely 1347 + 539, show extended emission on one side of the core (Perley 1982; Owen & Puschell 1984).

Although several sources, previously classified as one-sided, now appear to have lobes on both sides, the outer components either have significantly different surface brightness or are very asymmetrically located with respect to the core. It is also interesting to note that for the 13 sources with extended emission, the average value of the fraction of emission from the core at λ6 cm is ~ 0.5, which is much larger than the corresponding value for a complete sample of sources selected at a low frequency (*cf.* K81).

Acknowledgements

It is a pleasure to thank Chris Salter who made a significant number of the maps presented here. His help and advice during the course of this work has been invaluable. We also thank the NRAO staff for help in the observations. The National Radio Astronomy Observatory is operated by Associated Universities, Inc., under contract with the National Science Foundation.

References

Baars, J. W. M., Genzel, R., Pauliny-Toth, 1.1. K., Witzel, A. 1977, *Astr. Astrophys.,* **61,** 99.
Bentley, M., Haves, P., Spencer, R. E., Stannard, D. 1976, *Mon. Not. R. astr. Soc,* **176,** 275.
Bridle, A. H., Davis, M. M., Fomalont, E. B., Lequeux, J. 1972, *Astr. J.,* **77**, 405.
Bridle, A. H., Fomalont, E. B., Cornwell, T. J. 1981, *Astr. J.,* **86,** 1294.
Browne, I. W. A., Orr, M. J. L, Davis, R. J., Foley, A., Muxlow, T. W. B., Thomasson, P. 1982, *Mon. Not. R. astr, Soc,* **198,** 673.
Clements, E. D. 1983, *Mon. Not. R. astr. Soc,* **203,** 861.
Cohen, A. M., Porcas, R. W., Browne, I. W. A., Daintree, E. J., Walsh, D. 1977, *Mem. R. astr. Soc,* **84**, 1.
Conway, R. G., Davis, R. J., Foley, A. R., Ray, T. P. 1981, *Nature,* **294,** 540.
Douglas, J. N., Bash, F. N., Torrence, G. W., Wolfe, C. 1980, *Univ. Texas Publ. Astr.,* No. 17.
Edwards, T., Kronberg, P. P., Menard, G. 1975, *Astr. J.,* **80,** 1005.
Fanaroff, B. L., Riley, J. M. 1974, *Mon. Not. R. astr. Soc,* **167**, 31P.
Fanti, C, Fanti, R, Formiggini, L., Lari, C, Padrielli, L. 1977, *Astr. Astrophys. Suppl. Ser.,* **28,** 351.
Fanti, R, Feretti, L., Giovannini, G., Padrielli, L. 1979a, *Astr. Astrophys. Suppl. Ser.,* **35,** 169.
Fanti, R, Feretti, L, Giovannini, G., Padrielli, L. 1979b, *Astr. Astrophys.,* **73,** 40.
Feretti, L., Giovannini, G., Parma, P. 1982, *Astr. Astrophys.,* **115,** 423.
Haslam, C. G. T. 1974, *Astr. Astrophys. Suppl Ser.* **15,** 333.
Hewitt, A., Burbidge, G. 1980, *Astrophys. J. Suppl. Ser.,* **43,** 57.
Hintzen, P., Ulvestad, J., Owen, F. 1983, *Astr. J.,* **88,** 709 (HUO).
Jenkins, C. J., Pooley, G. G.. Riley, J. M. 1977, *Mem. R. astr. Soc,* **84,** 61.
Joshi, M. N. 1981, *Mon. Not. R. astr. Soc,* **197,** 7.
Kapahi, V. K. 1979, *Astr. Astrophys.,* **74,** L11.
Kapahi, V. K. 1981a, *J. Astrophys. Astr.,* **2,** 43 (K81).
Kapahi, V.K.1981b, *Astr. Astrophys. Suppl. Ser.,* **43,** 381.
Kapahi, V. K., Schilizzi, R. T. 1979, *Nature,* **277,** 610.
Katgert-Merkelijn, J., Lari, G, Padrielli, L. 1980, *Astr. Astrophys. Suppl. Ser.,* **40,** 91.
Kühr, H., Nauber, U, Pauliny-Toth, I. I. K., Witzel, A. 1979, *Max-Planck-Institut für Radioastronomie Preprint,* No.55.
Kühr, H., Witzel, A., Pauliny-Toth,I.I. K., Nauber, U.1981, *Astr. Astrophys. Suppl. Ser.,* **45,**367.
Macdonald, G. H., Miley, G. K. 1971, *Astrophys. J.,* **164,** 237.
Marscher, A. P., Broderick, J. J. 1983, *Astr. J.,* **88,** 759.
Miley, G. K. 1971, *Mon. Not. R. astr. Soc,* **152,** 477.
Miley G. K., Hartsuijker, A. P. 1978, *Astr. Astrophys. Suppl. Ser.,* **34,** 129 (MH78).
Owen, F. N., Porcas, R. W., Neff, S. G., 1978, *Astr. J.,* **83,** 1009.
Owen, F. N., Puschell, J. J. 1984, *Astr. J.,* in press.
Peacock, J. A., Wall, J. V. 1982, Mon. *Not. R. astr. Soc,* **198,** 843.
Perley, R. A. 1981, in *Optical Jets in Galaxies: Proc. 2nd ESO/ESA Workshop,* ESA SP162, p. 77.
Perley, R. A. 1982, *Astr. J.,* **87,** 859.
Potash, R. L, Wardle, J. F. C. 1979, *Astr. J.,* **84,** 707.
Schilizzi, R. T., Kapahi, V. K., Neff, S. G. 1982, *J. Astrophys. Astr.,* **3,** 173.
Schwab, F. R.1980, in *Proc Int. Optical Computing Conf*., Ed. W. T. Rhodes: *Proc. Soc. Photo-opt. Instrum. Eng*., **231,** 18.

Simard-Normandin, M., Kronberg, P. P., Button, S. 1981, *Astrophys. J. Suppl. Ser.,* **46,** 239 (SKB81).
Simard-Normandin, M., Kronberg, P. P., Button, S.1982, *Astr. Astrophys. Suppl. Ser.,* **48,**137.
Simard-Normandin, M., Kronberg, P.P., Neidhöfer, J.1981,*Astr. Astrophys. Suppl Ser.,* **43,**19.
Stannard, D., Neal, D. S. 1977, *Mon. Not. R. astr. Soc,* **179,** 719.
Swarup, G., Sinha, R. P., Hilldrup, K. 1984, *Mon. Not. R. astr. Soc,* **208,** 813.
Tabara, H., Inoue, M. 1980, *Astr. Astrophys. Suppl. Ser.,* **39,** 379 (TI80).
Thompson, A. R., Clark, B. G., Wade, C. M., Napier, P. J. 1980, *Astrophys. J. Suppl. Ser.,* **44,**151.
Wardle, J. F. C, Kronberg, P. P. 1974, *Astrophys. J.,* **194,** 249.
Wilkinson, P. N. 1982, in *IAU Symp.* 97: *Extragalactic Radio Sources,* Eds D. S. Heeschen & C. M. Wade, D. Reidel, Dordrecht, p. 149.
Wilkinson, P. N., Richards, P. J., Bowden, T. N. 1974, *Mon. Not. R. astr. Soc,* **168,** 515.